ISSN 0280–5316
ISRN LUTFD2/TFRT--5560--SE

Modelling and Control of an Electric Arc Furnace

Rui Pedro Paiva

Department of Automatic Control
Lund Institute of Technology
June 1996

Department of Automatic Control
Lund Institute of Technology
Box 118
S-221 00 Lund Sweden

Document name
Master Thesis

Date of issue
June 1996

Document Number
ISRN LUTFD2/TFRT--5560--SE

Author(s)
Rui Pedro P. C. Paiva

Supervisor
Mikael Johansson
Karl-Erik Årzén

Sponsoring organisation
Institute of Applied Mathematics, ITM

Title and subtitle
Modelling and Control of an Electric Arc Furnace

Abstract

In an Electric Arc Furnace (EAF), electrical energy is the main source of power used when melting scrap. In order to optimize the power consumption, the EAF must be properly understood. Also, since the main source of power are the electric arcs, its electrical and thermal properties must be analyzed. The arc power depends on its length and it is adjusted by moving the electrodes. In order to maintain the desired power levels, efficient control of the electrode movements is required.

This thesis presents an object-oriented model of the EAF where its main subsystems, namely the electrical system, the electrode positioning dynamics and the disturbances are analyzed separately. Furthermore, a fuzzy P-like impedance controller, based on the model implemented, is also presented.

Key words
Electric Arc Furnace, Object-Oriented Modelling, Computer Simulation, Fuzzy Control

Classification system and/or index terms (if any)

Supplementary bibliographical information

ISSN and key title
0280–5316

ISBN

Language
English

Number of pages
69

Recipient's notes

Security classification

Contents

Acknowledgments 2

1. Introduction 3
- 1.1 Outline of the thesis 4

2. The Electric Arc Furnace Process 6
- 2.1 The furnace 6
- 2.2 The steel-melting process 6

3. The Electric Arcs 8
- 3.1 Arc regions 8
- 3.2 Classification of electric arcs 9
- 3.3 AC electric arcs in an EAF 10
- 3.4 An AC arc model 15

4. Modelling the EAF System 19
- 4.1 A block diagram of the electrical system 19
- 4.2 The EAF electrical system 19
- 4.3 The electrode positioning system 22
- 4.4 The metal bath 24
- 4.5 The disturbances in the furnace operation 24
- 4.6 The interaction effect between the electrodes 24

5. Model Simulations 26
- 5.1 The electric arcs 26
- 5.2 The interaction effect 37
- 5.3 The effect of disturbances 39

6. The EAF Controller 45
- 6.1 Power control 45
- 6.2 Impedance control 46
- 6.3 A Fuzzy P-like impedance controller 47
- 6.4 Hydraulic control 49
- 6.5 Measurements 50
- 6.6 Control simulations 52

7. Conclusions 56
- 7.1 Contributions of the thesis 56
- 7.2 Limitations of the thesis 56

8. Bibliography 57

A. Köhle's model 58
- A.1 Relating Cassie's and Köhle's models 58
- A.2 The effect of changes in the arc length in Köhle's model 58

B. Simulation parameters 61

C. Dymola libraries 64
- C.1 Dynamic model library 64
- C.2 Steady-state model library 66
- C.3 Controller 68

Acknowledgments

First of all, I would like to thank my supervisors Mikael Johanson and Karl-Erik Årzén at LTH for all the help given. It want to thank especially Mikael for all the support, suggestions and motivation given during this period. I am also grateful to Hilding Elmqvist and Dag Brück, at Dynasim AB, for the help provided with Dymola. I would also like to thank Fredrik Norlund, at ABB Industrial Systems AB, for the data given and Ole Abildgard, at DDS AB, for the helpful written information. Finally, a word to the staff at LTH, who made my stay at the department very comfortable and pleasant.

Lund, June 1996

Rui Pedro Paiva

1. Introduction

In the steel industry, electric arc furnaces (EAF) are used to melt scrap into liquid steel. For the metallurgical reactions to take place, it is essential to achieve high temperatures in the furnace. In order to generate the necessary temperatures, electric arcs are used. The arcs consume a lot of electrical energy and, thus, there is a need to optimize the power delivered to the furnace. The arc power depends on the arc length, which is adjusted by means of the electrode positioning system. As a consequence, efficient control of the electrode movements is essential, so that the desired power level is achieved.

The topic of this thesis is modeling and control of electric arc furnaces. Physical modeling of the electric arc furnace serves two purposes.

- It allows us to gain knowledge about the EAF and, particularly, the electric arcs. Understanding the thermal and electrical properties of the arcs is essential to understanding the EAF and the steel-melting process.
- Simulation of different control strategies can be performed based on the model implemented.

In this thesis, object-oriented modeling was the method used to model the EAF. In this method, each component is modeled individually. The main reasons to use object-oriented modeling were the following.

- A modular structure is achieved.
- The model is easy to re-configure. Different furnaces have, for instance, different electrode positioning systems, transformers and metal properties. Object-oriented modeling makes it possible to change each component separately without changing the overall structure of the process. This situation is typical in real furnaces.
- In order to develop an object-oriented model, good software support is needed. In our model, the dynamic modeling environment, $Dymola^{TM}$, was used. This object-oriented language allows hierarchical decomposition of the models into submodels and reuse of the objects defined. The equations, typically differential and algebraic equations, are solved symbolically or to reduced Differential-Algebraic system of Equations (DAE).

The simulations performed show good correspondance with results reported in literature.

The second purpose of the thesis is to control the EAF electrical system. Some points are discussed, as follows.

- The control strategy consists of several levels, namely power, impedance and hydraulic control.
- The primary aim was to design an impedance controller. A fuzzy controller of P-type was implemented.

- The behavior of the controller was simulated and reasonable performance was achieved.

From the work developed, some conclusions were obtained.

- It is indeed possible to develop an object-oriented model of the EAF.
- More process knowledge in combination with identification experiments are needed for verification and model improvements.
- An impedance controller with reasonable performance is implemented. However, other control strategies could also be used. Moreover, power and hydraulic control could be further analyzed.

1.1 Outline of the thesis

The outline of the thesis is as follows:

- **Chapter 2**
  This thesis begins by presenting the EAF and the steel-melting process. The main parts of the EAF and the furnace operation are briefly described.
- **Chapter 3**
  In order to understand the furnace operation it is essential to understand the electric arcs. This chapter gives a general explanation of the thermal and electrical properties of the electric arcs. An electric arc model, proposed by Cassie is presented.
- **Chapter 4**
  Modelling the EAF is the topic of Chapter 3 and constitutes the most important part of the thesis. Models of the electric arc, furnace electrical system, electrode positioning dynamics and disturbances are implemented and discussed.
- **Chapter 5**
  In this chapter, simulations based on the model presented are performed. The different arcing conditions, the interaction effect between phases and effect of disturbances were simulated.
- **Chapter 6**
  Chapter 6 presents the control structure used. Power control and hydraulic control are discussed to some extent. Impedance control is analyzed in more detail. In this chapter, a fuzzy P-like controller is presented.
- **Chapter 7**
  Finally, some reflections on the work developed are made. The main contributions and limitations of the thesis are analyzed and directions for future work are suggested.
- **Appendix A**
  Appendix A describes in further detail a linear arc model proposed by Köhle. Its relation with Cassie's model is also analyzed.

- **Appendix B**
  This appendix gives the simulation parameters used in the models implemented. Some considerations regarding the way they were obtained are made.

- **Appendix C**
  The Dymola code developed for each model is presented in this appendix. A C function implemented for the fuzzy controller is also given.

2. The Electric Arc Furnace Process

An electric arc furnace is a device used in the steel industry to melt scrap and sometimes recycled steel into liquid steel. In order to provide the high temperatures, essential to the metallurgical reactions, electric arcs are used. The electric arcs are the main source of consumed electric energy in the EAF. A general description of them will be presented in Chapter 3.

2.1 The furnace

The main elements present in this three-phase open-arc furnace are the electrodes, the lance for oxygen blowing, the slag door and the tap hole, according to Figure 2.1 [Jansson, 1995].

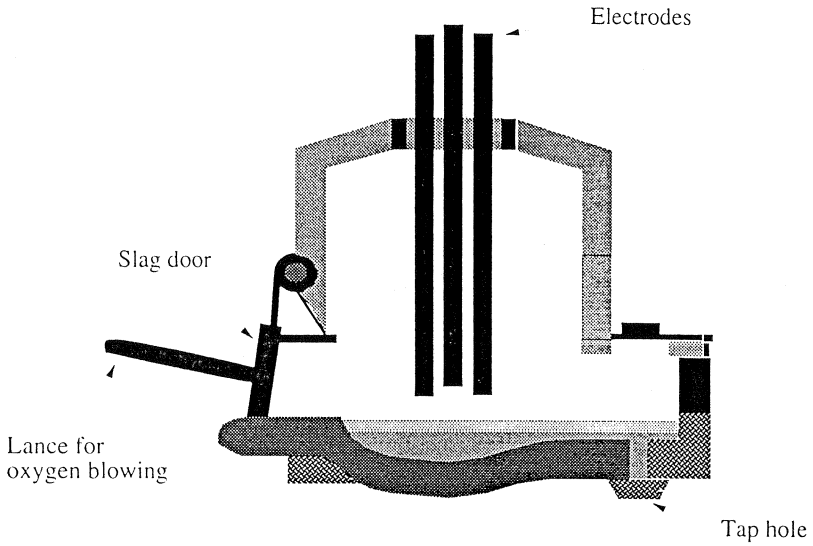

Figure 2.1 The electric arc furnace

The **three electrodes**, made of graphite and with a diameter of approximately 600 mm, are the main source of electrical energy to the melting process. Three arcs burn between the electrodes and the more or less molten metal bath. In order to adjust the arc length the electrodes are vertically adjustable.

2.2 The steel-melting process

The materials used in an EAF to produce steel are different types of scrap. In the first phase of the melting the raw materials are melted-down to hot metal which is tapped through the tap hole and then transported to further processing.

The melting process uses electricity as the most important energy source. As the process consumes a lot of electrical energy there is a need to fully utilize

the furnace. To attain better utilization two or more baskets of materials are melted in a row. The first one contains around 70 tons of scrap. When loading this basket anthracite and lime are also added. Together with the scrap, these materials produce a **layer of slag** on the top of the melt, which protects the refractory parts in the furnace. This layer also contributes to energy saving because it keeps the heat in the melt. The slag is removed later through the slag door.

When there is enough room for the next basket, this one, with around 50 tons, is loaded. If the charge has more baskets the procedure is repeated in the same way. After the last basket is loaded the purpose is to melt all the scrap to metal. The total process takes more or less 60 minutes.

A point that must be taken in account is the fact that, at the end of the melting process, when most of the scrap is melted, the arcs can affect the walls of the furnace which can cause expensive repair work. To avoid this, oxygen is blown into the bath using the oxygen lance. The combination of carbon and oxygen produces a **foaming slag** which is used as the protection mechanism. Another advantage of the oxygen blowing is the fact that its reaction with the oxidizing elements, such as carbon and iron, provides additional energy.

In the furnace, there are also **oil burners** used to generate homogeneous heat. In fact, the heat generated by the arcs is not uniform in all the scrap. Therefore, the oil burners are used in the cold spots during the first 4 or 5 minutes of each basket.

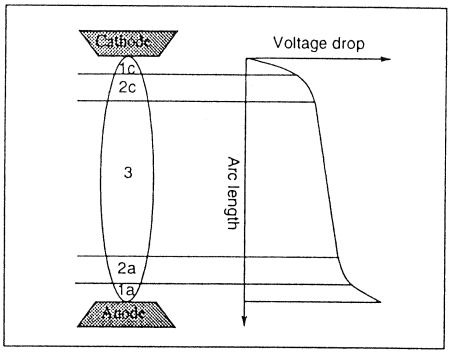

Figure 3.1 The potential distribution in an electric arc

3. The Electric Arcs

The electric arcs are used to provide the high temperatures necessary for the melting process. Thus, to be able to understand the operation of electric arc furnaces, it is essential to understand the nature of electric arcs. The aim of this chapter is to give an overview of electrical and thermal properties of electric arcs. Most of the material in this chapter is based on [Valderhaug, 1992], which is a good reference for a more in-depth treatment of electric arcs.

The way the electric arcs are formed can be briefly explained as follows. In the presence of an electric field, the gaseous medium between two electrodes is ionized producing an electrical conductance. Depending on the strength of the applied field and the characteristics of the electrodes and the medium, an electrical discharge is produced. The discharge is sustained by the current flowing in the gaseous medium and constitutes the **electric arc**.

3.1 Arc regions

In an electric arc, its physical, thermal and electrical properties are not uniform all over the arc. However, regions with similar characteristics can be found. A better understanding of the arcs is achieved by analyzing separately these regions.

Figure 3.1 shows that the voltage drop is nearly linear in the major part of the arc and so, in that region, the electric field strength is almost constant. Near the electrodes the field strength is much higher.

Based on the potential distribution of a DC arc, it can be divided into physically different regions. These are:

1. **The electrode regions**
   The electrode regions contain the *cathode* and *anode regions*. Both of them consist of:
   - **the sheath**
     This is the part of the the discharge which contains the electrode surface.
   - **the fall zones** (1c and 1a)
     The *cathode fall* and the *anode fall* are the regions immediately

in front of the electrodes surfaces. These zones correspond to the transition between metallic and gaseous plasma conduction. Due to the production and transport of space charges the field strengths are considerable in these regions.

- **the transition zones** (2c and 2a)
  In the *cathode transition zone* and the *anode transition zone* there are strong gradients of plasma properties such as temperature, potential, particle densities, current densities and radiation.

2. **The arc column** (3)
   The arc column is the main part of the arc and consists of the plasma between the anode and cathode regions. A plasma can be defined in a simple way as a "luminous conducting gas".
   In the arc column the thermal and electrical conditions are almost homogeneous: the temperature and field strength in the axis are almost constant. The field strength is small. The potential drop is nearly linear as referred above.

3.2 Classification of electric arcs

As the behavior of an electric arc depends on its size, power dissipation, current and external conditions it is useful to have a classification based on these aspects.

Our attention will be focused on the kind of arcs we can have in an electric arc furnace, namely *high-pressure*, *high* or *ultra high-current*, *high-power* and *free-burning* arcs.

According to *pressure*, the arcs can be divided in **high-pressure arcs** or low-pressure arcs. High-pressure arcs are the ones operating at pressures equal or above the atmospheric pressure. They attain approximately thermodynamic equilibrium.

The *current* also influences the behavior and characteristics of the arc. In an EAF we can have both **high-current arcs** and **ultra high-current arcs**. In high-current arcs, the currents are between 1kA and 10 kA. If arc current exceeds 10kA the arcs are denoted ultra high-current arcs.

According to *power dissipation* an arc can be classified as a low-power arc, high-power arc or ultra high-power arc. In an EAF we can have **high-power arcs**. In these kind of arcs the power dissipation originates a complex interaction between the arc and its surroundings: high radiative energy transfer, electrode melting and self-magnetic effects are typical phenomena present in high-power arcs.

The *conditions in the arc boundaries* can influence the arc "stability", i.e., the ability of the arc to keep in a given stable position. In an EAF we have **free-burning arcs** which are characterized by the fact that they don't have an imposed stabilizing mechanism. However, the interaction of the high current densities in the electrode region with its own magnetic field produces a Lorentz force field. The result of this force field is that the cathode region takes air from its surroundings and ejects it towards the anode inducting *free-convection effects* which stabilize the arc. That's the reason why these arcs

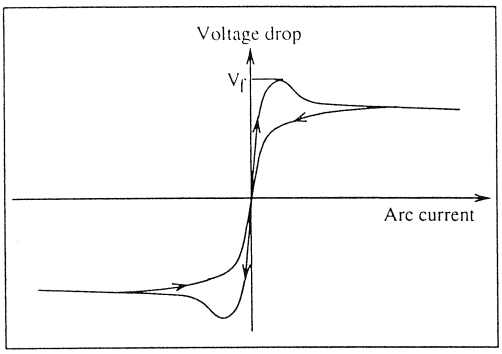

Figure 3.2 The dynamic current-voltage characteristic

are also called **self-stabilized arcs**.

After these general considerations concerning the arc regions and classification it is now time to describe the behavior of AC arcs.

3.3 AC electric arcs in an EAF

In an EAF the arcs burn between graphite (or carbon) electrodes and the surface of a more or less molten metal bath. As a consequence of the the AC operation mode the polarity of the arc changes. Thus, there is an alternation of the burning direction: from the electrode towards the metal pool and vice-versa.

As stated in Section 2.1, our EAF is a three-phase open-arc furnace where three arcs burn between the electrodes and the molten metal.

One representation of the dynamic characteristics of electric arcs is the **current-voltage characteristic** (Figure 3.2). From this figure, we see how an increasing current is accompanied by an increasing arc voltage. When the arc voltage exceeds the firing voltage V_f, the field strength between the electrode and the bath is large enough to ignite the electric arc. Due to Joule heating the arc gets more ionized and the arc conductance increases resulting in a decreasing arc voltage. As in electric arc furnaces we have high or ultra-high currents, the current-voltage characteristic is almost flat. The arc responds to the high energy losses with an increase of the field strength. This increasing in the field strength conjugated with the falling trend of voltage due to increasing arc conductance with current, qualitatively explains that flatness. When the current goes down towards zero, the voltage also decreases and the *arc is extinguished*. Then, the cycle begins with reversed polarity.

The phenomenon described above corresponds to a typical arc. However, the arcing conditions change during the furnace operation. According to [Timm and Grigat, 1987], in the beginning of the process the arc surroundings are "cold" and there is a large stochastic disturbance manifested by random changes in the arc lengths due to scrap falling. As a consequence, the arcs are noisy and the current and voltage waveforms are strongly distorted. Furthermore, the arc is unstable in the sense that there are time intervals in which it doesn't ignite. Around 7 minutes later, the arc surroundings are warmer and the disturbances are not so large. The arc becomes less noisy and the

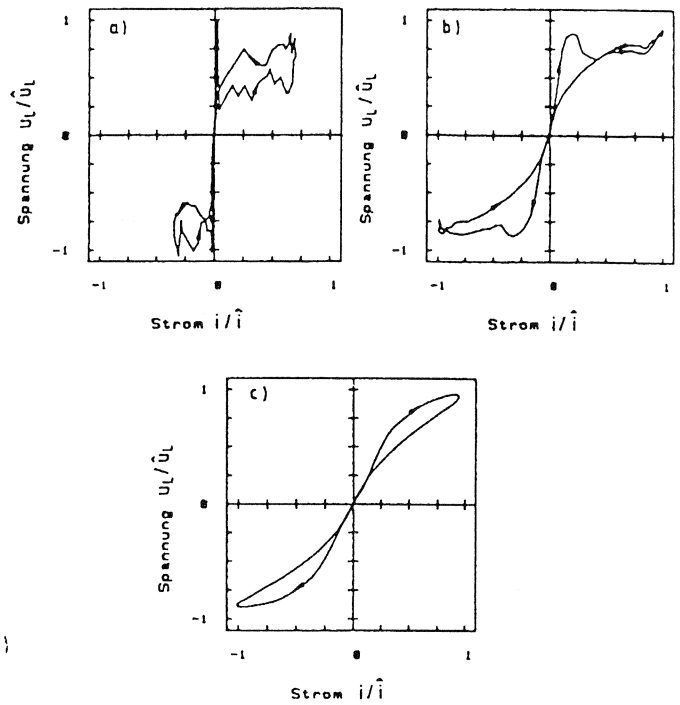

Figure 3.3 The dynamic current-voltage characteristics in the beginning of the process, 7 minutes after and 27 minutes after

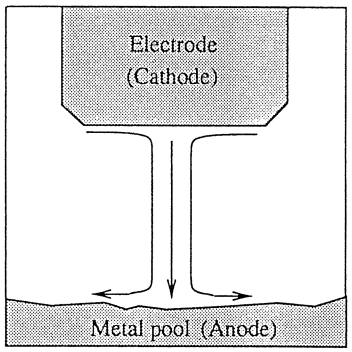

Figure 3.4 The arc flow in the negative polarity mode

currents and voltages are less distorted. After more or less 27 minutes the arc surroundings are "hot" and there are almost no disturbances. The arc becomes almost linear and the distortion in the current and voltage waveforms is strongly reduced. Figure 3.3, adopted from [Timm and Grigat, 1987], presents the dynamic current-voltage characteristic in the situations described.

Depending on the electrical polarity there are two different regimes of the arc behavior: in the negative polarity mode the electrode acts as the cathode while in the positive polarity mode that role is played by the metal pool. As a consequence, the arc properties will differ considerably when the polarity changes.

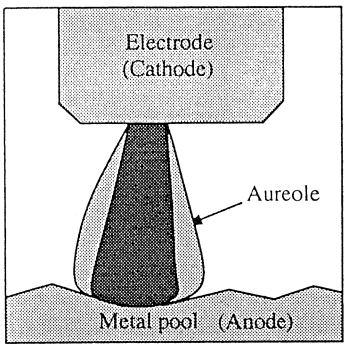

Figure 3.5 The electric arc in the negative polarity mode

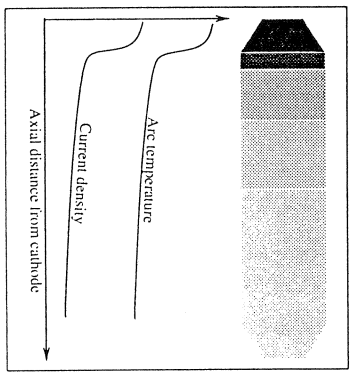

Figure 3.6 Axial current density and temperature distribution in the arc

The electrode as cathode

The electrode working as cathode is called the *negative polarity mode*. In this mode the arcing can be described as follows. The arc ignition takes place at the lowest point of the electrode tip. As the current rises the arc diameter increases. Furthermore, the arc starts to move at the electrode surface and a plasma jet (due to the the free-convection effects referred in Section 3.2) develops in the cathode region. As the current decreases, the arc intensity and diameter decreases and when the current is zero, the arc is extinguished.

Due to the free-convection effects there is a *flow field* induced by the electromagnetic pumping force. In figure 3.4 we see that the flow enters the arc core from its periphery and flows towards the anode. The arc axial velocity has its maximum near the cathode. Towards the arc column it decreases rapidly and it's almost constant along the axis in the arc column. Reaching the anode, the axial velocity has a sharp drop which produces a *stagnation layer* in front of the anode. Figure 3.5 shows that the arc is strongly contracted near the cathode and it spreads towards the anode due to the stagnation layer.

The arc temperature takes its maximum value in front of the cathode due to Joule heating and goes down as the arc spreads.. The temperature is almost constant along the arc axis (Figure 3.6). In terms of its radial distribution it can be seen in Figure 3.7 that it is high and nearly constant in the core and drops sharply in the fringes.

The *current density* is very high near the cathode tip due to the massive production of charges. It decreases rapidly towards the arc column due to temperature decrease, according to Figure 3.6. Its radial distribution is com-

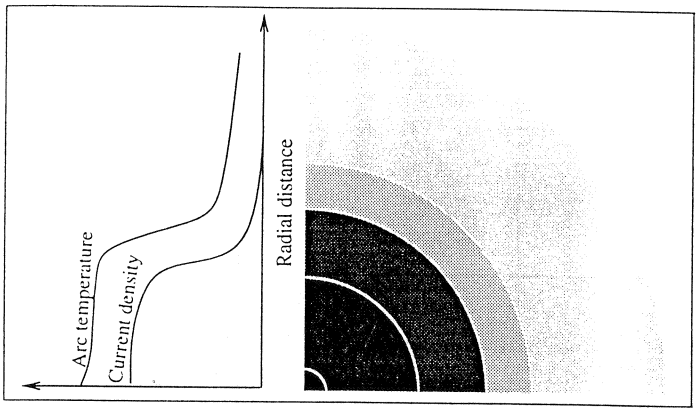

Figure 3.7 Radial current density and temperature distribution in the arc

parable to the one of the temperature: higher in the core and dropping sharply in the fringes.

Now, let's see what happens in the cathode, arc column and anode.

1. **The cathode**
   At the cathode region strong, self-induced plasma jets are directed towards the anode surface with velocities higher than 1000 m/s. The vapor jets due to high energy dissipation at the electrode have velocities that can reach 10000 m/s.

2. **The arc column**
   In this polarity mode, the behavior of the arc is comparable to a free-burning DC arc.

   A *thermal layer* (the aureole in Figure 3.5) is formed due to energy loss from the plasma column: the surrounding gas is heated by convection and absorption of the radiation. The major net energy losses are *convection* due to plasma flow (50 - 70%), *radiation* (20 - 40%) and *thermal conduction* (< 10%). In the core of the arc there are considerable radiation losses, due to its higher temperature. This energy is absorbed by the outer regions. The convective losses occur mainly in the peripheral regions and they transport away the energy gained by conduction and radiation.

   Apart from flow fields, there is another important cathode flow phenomena, namely *vapor jets*. Vapor jets have their origin in the vaporization of electrode materials in the cathode region and have an important influence on the arc behavior. The electrode evaporation is a consequence of the heating of the electrode materials. If the electrode is cooled we'll see little or no vaporization even at high currents. But if the electrode is only weekly cooled, the electrode erosion increases strongly with the current. Small particles detach from the electrode and accelerate along the axis. As the current increases, the erosion becomes large enough to generate a jet from the electrode towards the column. As the vaporized materials have a lower ionization potential than the gas, they will considerably influence the plasma properties. If the evaporation of the electrode is very strong, **arc instability** may occur due the mobility of the arc root which induce unstable column behavior.

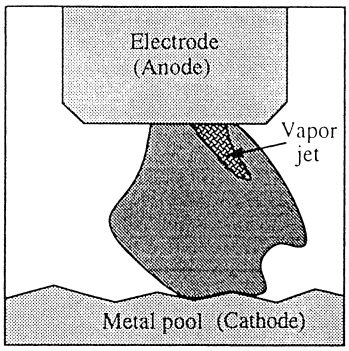

Figure 3.8 The electric arc in the positive polarity mode

In summary, the conduction radius in the arc column is large (up to 30 cm), the current density is low ($1000 A/cm^2$), the field strength is low (up to 10 V/cm) and the temperature is high ($> 10000 K$).

3. **The anode**
   Near the anode, the plasma jet velocity slows down forming a stagnation layer, as referred above. The arc tries to make holes in the liquid metal but its strength is distributed to a large area.

The other regime we can have is the electrode as anode.

The electrode as anode

The electrode operating as anode is called the *positive polarity mode*. In this mode we have a very complicated unstable arc. The flows, geometry, power balance and other properties of the arc are very different from the ones of the opposite regime.

1. **The cathode**
   In the metal bath, strong and unstable vapor jets can be directed to the electrode. The cathode spots are unstable and highly mobile.

2. **The arc column**
   The core of the arc is usually contorted and highly mobile. Due to magnetic instability it has *sideway velocities* that can reach 600 m/s and result in significant convection losses.

   The arc column is much broader near the electrode compared to the other regime which results in an increased heat of the electrode and a decreased direct heat transfer due to higher energy dissipation.

   There can also be a strong plasma flow from the anode electrode towards the cathode.

3. **The anode**
   As can be seen in Figure 3.8, the anode spot is much larger than in the opposite polarity mode. In the same figure we see that weak jets are developed from the electrode. However, these jets are not strong enough strength to stabilize the arc column.

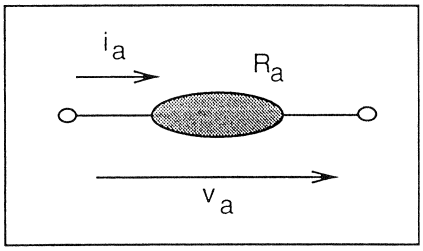

Figure 3.9 The electrical arc as a circuit element

3.4 An AC arc model

In this section an empirical model of the arc column will be presented. As will be seen, this model does not describe the anode and cathode regimes and so, a separate description of these will be given. The measurements made in a typical arc furnace control system are sampled by around 3 Hz and do not capture the phenomena described below. Thus, a simple linear arc model will also be presented.

A model of the arc column

One of the most common empirical models of AC arcs is **Cassie's model** [Browne, 1955]. It describes the arc as an electric circuit element characterized by the *arc voltage* v_a, the *arc current* i_a and the *arc resistance* R_a(Figure 3.9).

In this model, three assumptions are made. First, it is assumed that the change with time in the *inner energy* $\hat{U}_a(t)$ is equal to the difference between the electrical *power input* per length unit $\hat{P}_{in}(t)$ and the *power dissipation* per length unit $\hat{P}_{out}(t)$:

$$\frac{d\hat{U}_a(t)}{dt} = \hat{P}_{in}(t) - \hat{P}_{out}(t) \tag{3.1}$$

With $E_a(t)$ as the electrical field strength, the electrical power input is:

$$\hat{P}_{in}(t) = E_a(t)i_a(t) \tag{3.2}$$

The field strength is equivalent to the voltage drop per length unit. It follows that:

$$\frac{d\hat{U}_a(t)}{dt} = E_a(t)i_a(t) - \hat{P}_{out}(t) \tag{3.3}$$

The last assumption is that the arc conductance $\hat{G}_a$ is proportional to its inner energy:

$$\begin{aligned} \hat{G}_a(t) &= g_0\hat{U}_a(t) \\ g_0 &= \text{constant} \end{aligned} \tag{3.4}$$

The power dissipation per length unit is described as:

$$\hat{P}_{out}(t) = E_0(t)i_a(t) = E_0(t)^2\hat{G}_a(t) \tag{3.5}$$

where the constant E_0 can be seen as the electric field in a corresponding static arc. Substituting Eqs. 3.4 and 3.5 in Eq. 3.3 we obtain the **Cassie model**:

$$\frac{1}{\hat{G}_a(t)}\frac{d\hat{G}_a(t)}{dt} = \frac{1}{\tau_a}\left[\left(\frac{E_a(t)}{E_0}\right)^2 - 1\right] \tag{3.6}$$

There, τ_a is a time constant that characterizes the arc dynamics:

$$\tau_a = \frac{1}{g_0 E_0^2} \tag{3.7}$$

Inserting in 3.6 the *arc resistance* per unit length, $\hat{R}_a(t)$, it yields:

$$\frac{d\hat{R}_a(t)}{dt} = \frac{1}{\tau_a}\left[1 - \left(\frac{E_a(t)}{E_0}\right)^2\right]\hat{R}_a(t) \tag{3.8}$$

and therefore the total arc column resistance is given by:

$$R_a(t) = h_a(t)\hat{R}_a(t) \tag{3.9}$$

and where h_a is the *arc length*. The main advantage of this model is its simplicity: only two equations (Eqs. 3.8 and 3.9) and two parameters (the time constant and the electric field strength) which should be easy do adjust. The main limitation is the fact that the model only describes the arc column electrical characteristics and does not take into account the voltage drop in the cathode and anode regions.

A model of the anode and cathode regions

The cathode and anode voltages can be modeled in a simple way by considering them constant during the polarity half-periods:

$$v_A(t) = \begin{cases} v_{Ae}, & i_a(t) > 0 \\ v_{Am}, & i_a(t) < 0 \end{cases} \tag{3.10}$$

$$v_C(t) = \begin{cases} v_{Cm}, & i_a(t) > 0 \\ v_{Ce}, & i_a(t) < 0 \end{cases} \tag{3.11}$$

where v_{Ae}, v_{Am}, v_{Cm} and v_{Ce} are the anode and cathode voltages in the different modes. This is an ideal representation and so we have to consider more complex dynamic phenomena. In fact, in the polarity inversion there is *hysteresis effect*: the voltage drop, both in the electrode and in the metal pool depends not only on the current but also on whether it is increasing or decreasing. Figure 3.10 illustrates this phenomenon in the electrode.

A capacitive effect occurs near current zero and so the anode and cathode voltages will change towards the voltages corresponding to the opposite polarity with some connected time constant. Thus, the anode and cathode voltages in the electrode and metal pool can be described as:

$$\begin{aligned} v_e(t) &= \frac{v_{Ae} + v_{Ce}}{2} + \frac{v_{Ae} - v_{Ce}}{2} \cdot \tanh(\tau_e[i_a(t) - \Delta i_{ae}(t)]) \\ v_m(t) &= \frac{v_{Am} + v_{Cm}}{2} + \frac{v_{Am} - v_{Cm}}{2} \cdot \tanh(\tau_m[i_a(t) - \Delta i_{am}(t)]) \end{aligned} \tag{3.12}$$

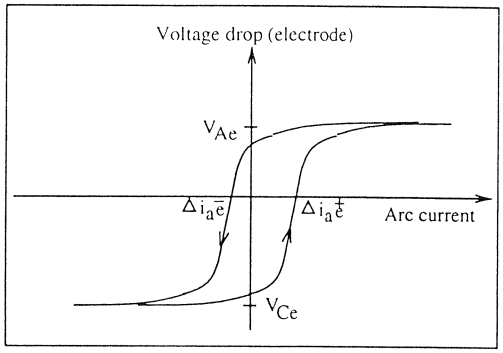

Figure 3.10 The hysteresis effect in the inversion of polarity

where τ_e and τ_m are the connected time constants of the electrode and metal pool, respectively, and Δi_{am} Δi_{ae} denote the current values for which the voltage alternate. These can be described in a similar way by:

$$\Delta i_{ae}(t) = \frac{\Delta i_{ae}^+ + \Delta i_{ae}^-}{2} + \frac{\Delta i_{ae}^+ - \Delta i_{ae}^-}{2} \cdot \tanh\left(\tau_{\Delta i}\frac{di_a(t)}{dt}\right)$$
$$\Delta i_{am}(t) = \frac{\Delta i_{am}^+ + \Delta i_{am}^-}{2} + \frac{\Delta i_{am}^+ - \Delta i_{am}^-}{2} \cdot \tanh\left(\tau_{\Delta i}\frac{di_a(t)}{dt}\right) \qquad (3.13)$$

where Δi_{ae}^+ and Δi_{ae}^- represent the current values for which the electrode voltage alternate, as can be seen in Figure 3.10, and Δi_{am}^+ and Δi_{am}^- are the same for the metal. The time constant $\tau_{\Delta i}$ is used to ensure a smooth transition between the referred current values.

So, we have for the total anode and cathode voltages:

$$v_A(t) + v_C(t) = v_e(t) + v_m(t) \qquad (3.14)$$

A complete model of the AC arc

Now, conjugating the arc column, the anode and the cathode models described above, we can present a complete model of the electric arc voltage:

$$v_a(t) = v_e(t) + v_m(t) + R_a(t) \cdot i_a(t) \qquad (3.15)$$

In this model, the arc is seen as a nonlinear resistance. As a consequence, its presence will cause distortion to the currents and voltages in the circuit. The distortion is manifested by harmonics to the original sinusoidal signals.

In order to have faster simulations, a steady-state model is required. As Cassie's model is not adequate to obtain a steady state model, another arc model will be presented.

A linear AC arc model: Köhle's model

In order to obtain a simpler arc model, Köhle proposed to represent the arc as an equivalent linear circuit element constituted by a resistive and a reactive part, as seen in Figure 3.11.

In his model, Köhle defines the arc reactance X_L as a function of its resistance:

$$X_L = aR_L + bR_L^2 \qquad (3.16)$$

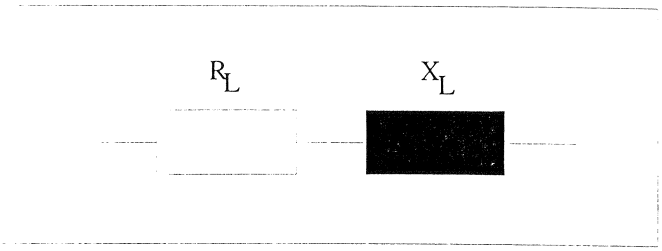

Figure 3.11 Köhle's model of the arc

where the first term represents the influences of low frequency fluctuations and the second represents the influences of harmonics.

As referred in [Köhle, 1992] the following typical values for a and b were obtained, based on performed measurements.

$$\begin{cases} a = 0.12 \\ b = 0.02 \end{cases} \tag{3.17}$$

However, it must be taken into account that those values vary during the melting process: they decrease from the beginning of the process until we have a flat bath. Thus, depending on the furnace conditions, we have the following values, according to [Köhle, 1992]:

$$\begin{cases} a = 0.2 & \text{, start} \\ a = 0.1 & \text{, main melting} \\ a = 0 & \text{, flat bath} \end{cases} \tag{3.18}$$

This decreasing of the parameters can be explained by the fact that the melting process is accompanied by a decrease of the resistance of the metal bath.

As a conclusion, this model does not capture the dynamic electrical properties of an electric arc. However, it captures the average arc characteristics and, thus, it is very useful for steady-state simulations, where getting the dynamic properties of the arc is not a main concern. A more detailed description of this model and its relation to Cassie's model is presented in Appendix A.

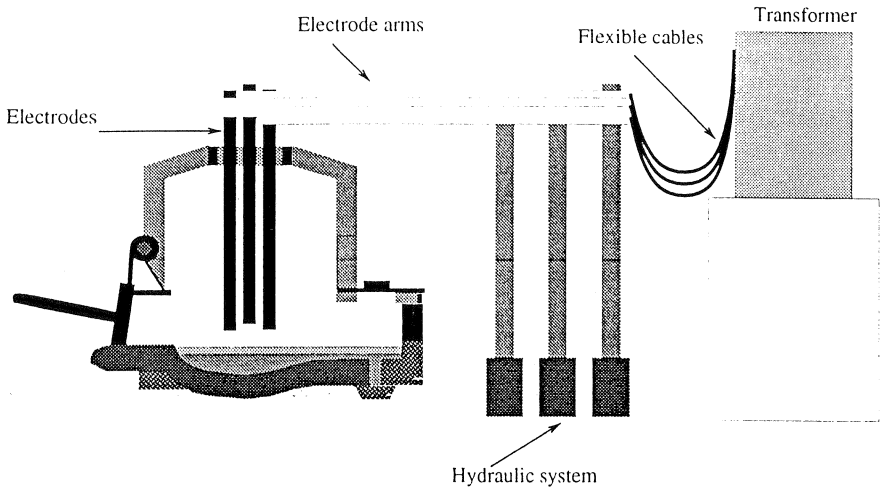

Figure 4.1 A block diagram of the EAF electrical system

4. Modelling the EAF System

The purpose of this chapter is to present a model of the furnace which describes the EAF electrical system, the electrode positioning system, the characteristics of the metal bath and the disturbances to the process.

4.1 A block diagram of the electrical system

Figure 4.1, adopted from [Jansson, 1995], presents a block diagram of the electrical system of a typical electric arc furnace.

The *three-phase transformer* is the source of electrical energy to the furnace. The primary voltage is nearly 20-30 kV and the secondary voltage can vary from 100 V to 800 V. The ratio of the primary to the secondary voltages is selected via a *tap changer* on the transformer. This device changes the number of coils in the primary side which allows the adjustment of the secondary voltage in discrete steps. This adjustment is carried out on the primary side due to the high currents in the secondary side. In the primary side, the transformer coils are star or delta connected while in the secondary side they are delta connected.

Flexible cables connect each phase of the transformer to the *electrodes*. These are supported by *electrode arms* which are mounted on a *hydraulic system* that allows vertical movements of the electrodes, necessary to adjust the arc length.

4.2 The EAF electrical system

In this section, an equivalent model of the furnace electrical system is presented based on equivalent circuit descriptions, i.e., taking into account the models of the generator, transformer, cables, electrodes, electric arc (as defined

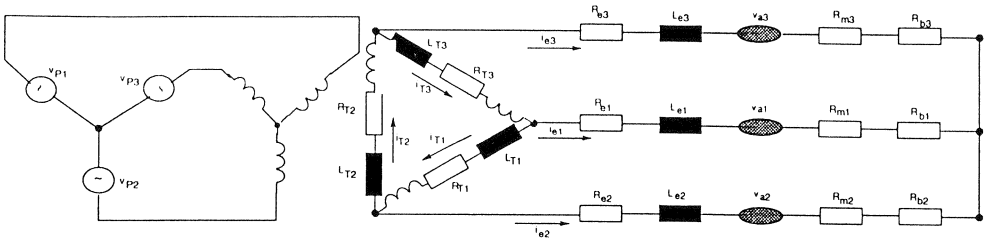

Figure 4.2 The equivalent circuit of the EAF

above) and other elements, in order to form a complete circuit. This circuit is represented in Figure 4.2, based on the fact that the transformer secondary side and the furnace circuit form an almost pure delta-star circuit.

The generator

The source of power to the EAF is a three-phase voltage generator in which perfect symmetry is assumed. Thus, the voltages v_{p1}, v_{p2} and v_{p3} have relative phase shifts of 120°, with the sequence P1-P2-P3:

$$\begin{aligned} v_{p1} &= V_P \sin(2\pi f t) \\ v_{p2} &= V_P \sin(2\pi f t - 2\pi/3) \\ v_{p3} &= V_P \sin(2\pi f t - 4\pi/3) \end{aligned} \tag{4.1}$$

where V_P is the common voltage amplitude, $f = 50Hz$ is the electrical frequency and t stands for time.

The transformer

The secondary coils of the transformer are delta connected and it's assumed that the primary ones are star connected.

In the model, R_{Ti} and L_{Ti} represent the resistances and inductances in the transformer and flexible cables. Its assumed that they are identical in the three phases:

$$\begin{aligned} L_{T1} = L_{T2} = L_{T3} = L_T \\ R_{T1} = R_{T2} = R_{T3} = R_T \end{aligned} \tag{4.2}$$

Analyzing the circuit we get the following expression:

$$R_{T1} i_{T1} + L_{T1} \frac{di_{T1}}{dt} + R_{T2} i_{T2} + L_{T2} \frac{di_{T2}}{dt} + R_{T3} i_{T3} + L_{T3} \frac{di_{T3}}{dt} = 0 \tag{4.3}$$

due to the fact that $v_{T1} + v_{T2} + v_{T3} = 0$. According to Eq. 4.2, it follows that:

$$R_T(i_{T1} + i_{T2} + i_{T3}) + L_T \left(\frac{di1}{dt} + \frac{di2}{dt} + \frac{di3}{dt} \right) = 0 \tag{4.4}$$

and furthermore:

$$\begin{aligned} i_{T1} &= i_{T3} - i_1 \\ i_{T2} &= i_{T1} - i_2 \\ i_{T3} &= i_{T2} - i_3 \end{aligned} \tag{4.5}$$

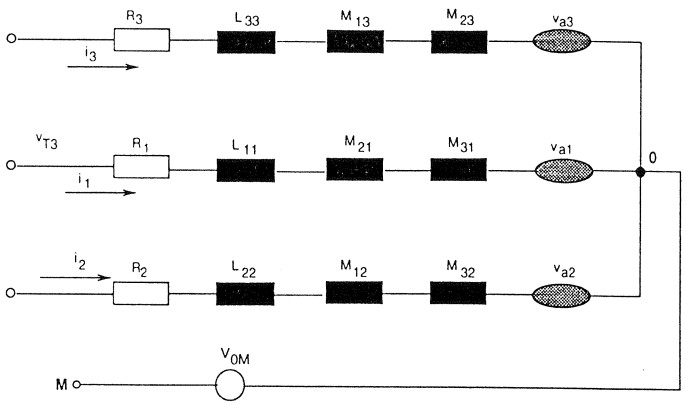

Figure 4.3 The EAF secondary circuit with self and mutual inductances

From the previous equations and according to the properties of three-phase systems, we can derive the following expression that relates explicitly i_i as a function of i_{Ti}:

$$|I_{T1}| = |I_{T2}| = |I_{T3}| \Longrightarrow |i_i| = \sqrt{3}|i_{Ti}| \tag{4.6}$$

The secondary circuit

For each phase i, R_{ei} and L_{ei} represent the electrode impedances, v_{ai} stands for the arc voltages, as described by Eq. 3.15, R_{mi} are the metal bath resistances which will be described later, and R_{bi} represents the charge bottom resistances in the furnace.

In the furnace there is also electrical conduction between the electrodes. However, since, according to [Valderhaug, 1992], these currents are nearly 1% of the phase currents, these direct electrode-electrode currents will be neglected.

In this model, the electrode self and mutual inductances between the phases are lumped together into variable electrode inductances. Thus, in Figure 4.3, a model illustrating *self* and *mutual inductances* is presented.

The notation used in this model is the following: R_i represents the phase resistances, L_{ii} stands for the self-inductances in each phase, M_{21} and M_{31} are the mutual inductances in phase 1 and the same for the other phases. It is assumed that the mutual inductances have the same effect in both directions:

$$\begin{aligned} M_{12} &= M_{21} \\ M_{23} &= M_{32} \\ M_{31} &= M_{13} \end{aligned} \tag{4.7}$$

Since perfect symmetry is assumed, it turns out that:

$$M_{12} = M_{23} = M_{31} \tag{4.8}$$

Some reflections on modelling of mutual inductances are presented in Section 4.6.

The arc voltages are denoted by v_{ai}. 0 denotes the electrical star-point, which corresponds to the metal bath. M represents the electrical neutral point,

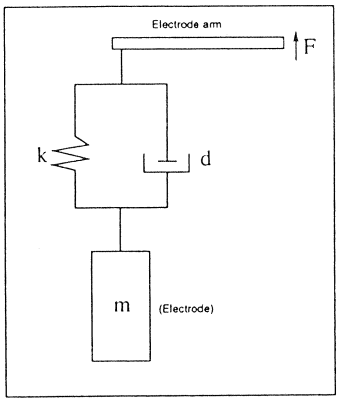

Figure 4.4 The electrode positioning system

which corresponds to the hearth of the furnace. The potential difference between the electrical star-point and the furnace neutral point is denoted v_{0M}.

From Figure 4.3 we can obtain the electrode-to-neutral voltages:

$$\begin{aligned} v_{1M} &= R_1 i_1 + L_{11}\frac{di1}{dt} + M_{21}\frac{di2}{dt} + M_{31}\frac{di3}{dt} + v_{a1} + v_{0M} \\ v_{2M} &= R_2 i_2 + L_{22}\frac{di2}{dt} + M_{12}\frac{di1}{dt} + M_{32}\frac{di3}{dt} + v_{a2} + v_{0M} \\ v_{3M} &= R_3 i_3 + L_{33}\frac{di3}{dt} + M_{13}\frac{di1}{dt} + M_{23}\frac{di2}{dt} + v_{a3} + v_{0M} \end{aligned} \tag{4.9}$$

Applying Kirchoff's current law at the star-point we get:

$$i_1 + i_2 + i_3 = 0 \tag{4.10}$$

Together, the equations presented above describe the EAF electrical system.

4.3 The electrode positioning system

If one want to obtain an efficient control system, it is very important to understand the mechanics of the hydraulic system that positions the electrodes. Since we don't have much information available concerning this point, we review a model presented in [Billings, 1981], which is said to be typical of many installations, and a model described in [Hauksdóttir *et al.*, 1995].

In [Billings, 1981], the servomechanism for positioning the electrodes consists of an amplidyne Ward-Leonard drive. The electrode mast dynamics are modeled as a combination of a mass, a spring and a damper, as in Figure 4.4. Thus, the dynamics of the electrodes are represented by a damped second-order system.

From this model we can derive the following equation:

$$m\ddot{x} = F + d\dot{x} + kx - mg \tag{4.11}$$

There, x represents the electrode position, F is the hydraulic force, d and k stand for the damper and spring constants, m is the electrode mass and g is the acceleration of gravity. Notice that the electrode mass changes, as electrode materials are consumed during the steel-melting process.

Due to the considerable weight of the electrodes, moving them upwards requires a much bigger force than in the opposite direction. As a consequence, when designing an electrode positioning controller, different gains should be used. This problem will be analyzed to some extent in Chapter 6.

In [Billings, 1981], it is suggested to estimate the values of the natural frequency and damping coefficient by means of accelerometers connected to the electrode tip.

In [Hauksdóttir *et al.*, 1995] a simple second-order model of the electrode positioning equipment is given by the following transfer function:

$$G_{EP}(s) = \frac{Ke^{-T_d s}}{(\tau s + 1)s} \tag{4.12}$$

where K is the gain factor, τ is a time constant and the exponential captures a delay of T_d seconds. The parameters of the electrode positioning transfer function were estimated using measurements in closed loop. The experiments described in [Hauksdóttir *et al.*, 1995] consisted of giving constant low and up signals for a specified amount of time and monitoring the response of the electrode positioning system. In this way, it was possible to estimate the average delay, gain and time constants of the electrode positioning system.

In our model, the electrode positioning dynamics are modeled as an integrator in series with a first order system:

$$\frac{h_a(s)}{v_{ref}(s)} = \frac{1}{s} \cdot \frac{1}{Ts + 1} \tag{4.13}$$

The reason why this structure is used will be given in Chapter 6. Another point is that, as the speed to move the electrodes is limited, a saturation is also included in the model. Typical values of electrode maximum speed are around $10cm/s$, according to data collected from the steel mill at Smedjebacken. Notice that the maximum upwards and downwards speed vary. A more complete model should include the hydraulic system. However, little knowledge of this subsystem is available. Therefore, due to the lack of knowledge and to the fact that our model captures the dynamics of the electrode positioning system, it can be used with enough accuracy.

The time constant T is calculated as follows. The settling time T_s is assumed to be 1 sec. Defining the final value as 98% of the nominal final value, we obtain:

$$T \simeq 0.25T_s = 0.25sec \tag{4.14}$$

In our model this transfer function is converted to state-space equations, so that it is possible to select the initial conditions.

4.4 The metal bath

During furnace operation, the characteristics of the bath change as the solid scrap melts into liquid steel, until we have a metal pool. This leads to large changes in the charge conductance. However, as these changes are slow, one approach is to describe the metal bath as a constant resistance and consider its conductance variation as a disturbance to the process. This is the approach taken in this work.

Another approach is to capture the changes in the metal bath by varying the parameters a and b in Köhle's model. As referred before, those parameters decrease during the furnace operation, which corresponds to the increase in the metal bath conductance.

4.5 The disturbances in the furnace operation

The main disturbance to the process is due to scrap movements, mainly in the beginning of the melt-down, when we don't have a liquid bath. In this phase the arc must be short, in order to attain the desired high power. As a consequence, some times the scrap touches the electrodes, which cause short circuits. Therefore, an efficient controller is required. To achieve this goal, it is important to treat the disturbances properly.

In both of the arc models, we can include the disturbances by varying the arc length which is essentially what happens due to scrap movements. A quantitative disturbance model should be based on furnace measurements. In [Hauksdóttir *et al.*, 1995], the disturbances are identified by keeping the three electrodes fixed and measuring the currents.

4.6 The interaction effect between the electrodes

In the EAF there is a strong coupling effect between the electrodes. This means that when we move one of them, the currents in the others also change. This is due to the nature of three phase system and also because of the mutual inductances between the phases. As the interaction effect is significant, it is important to include it in the model.

One good way to estimate the coupling effect is experimentally. Since in our case the required measurements are not available, a rough solution is to consider the mutual inductances as constant. According to [Billings, 1981] the interaction effect is less than 10% and, thus, we could pick a value that satisfies this condition.

An alternative and more appealing model is presented in [Valderhaug, 1992]. There, the current variations due to changes in the arc length are mod-

eled by the following equations:

$$\begin{pmatrix} \Delta i_{e1} \\ \Delta i_{e2} \\ \Delta i_{e3} \end{pmatrix} = H \cdot \begin{pmatrix} \Delta h_{a1} \\ \Delta h_{a2} \\ \Delta h_{a3} \end{pmatrix} \tag{4.15}$$

$$H = \begin{pmatrix} h_{11} & h_{12} & h_{13} \\ h_{21} & h_{22} & h_{23} \\ h_{31} & h_{32} & h_{33} \end{pmatrix} \tag{4.16}$$

where the matrix elements h_{ij} describe the effect of the electrode movements in the currents. These values depend on the short-circuit impedances and on the arc characteristics. The values of the matrix H were obtained experimentally by moving one electrode at a time and analyzing the corresponding changes in the electrode currents. These constitute a good approximation but it should be stressed that the results obtained depend on the furnace conditions and on the random disturbances.

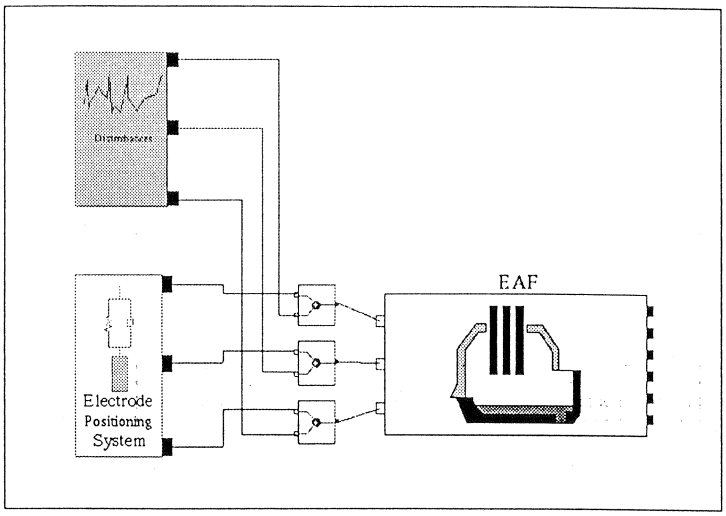

Figure 5.1 The diagram model used in Dymola

5. Model Simulations

In this chapter, some simulations based on the model presented will be performed. We will begin with dynamic simulations where Cassie's arc model is used. The goal of these simulations is to observe the transient behavior of arc currents, voltages and anode and cathode voltages for a specified arc length. Then, in order to analyze the coupling effect between the phases, steady-state simulations, for which Köhle's model is used, are made. In these simulations, one electrode is moved at a time and the current variations in the other phases are analyzed. Finally, the effect of the stochastic disturbances on the arc lengths is pointed out.

Data concerning short-circuit impedances, i.e., transformer and electrode impedances, were obtained from Fundia in Smedjebacken. Also, measurements of the secondary currents and voltages were available and were used to manually adjust the other parameters, so that the desired voltages and currents were obtained. Also data from [Valderhaug, 1992] was used. The parameters used are given in Appendix B. In order to have more accurate simulations further process knowledge, system identification and model validation are needed.

All the simulations were performed using the dynamic modeling language $Dymola^{TM}$ version 3.0 Final Beta. Figure 5.1 shows the diagram model used in Dymola. Please refer to Appendix C to view the source code used.

5.1 The electric arcs

In this section the simulations are performed using the dynamic model in Figure 5.2. This figure corresponds to the object EAF in Figure 5.1.

As described before, this model includes the furnace three-phase generator, transformer, electrode positioning system and secondary circuit. The arc was modeled according to Cassie and the inductances connecting the phases try to capture the effect of coupling. No disturbances are included so that the ideal phenomena can be visualized.

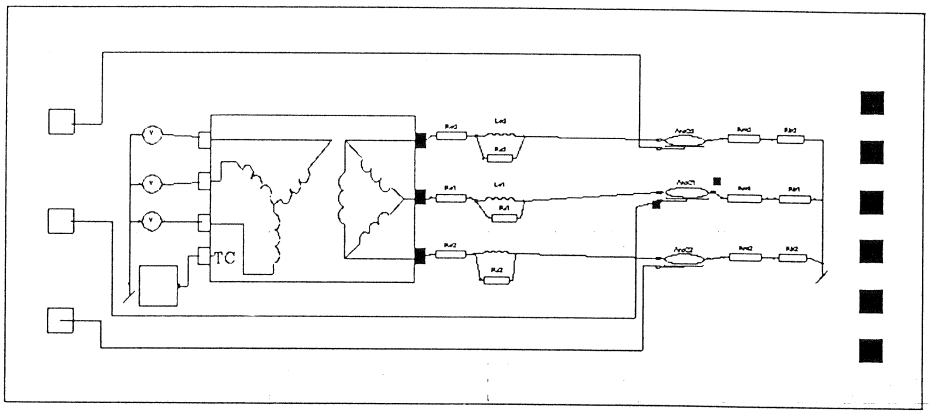

Figure 5.2 The EAF diagram for the dynamic model

When trying to run the model, a problem with the DAE index showed up. In order to solve it, we connected resistances in parallel with the electrode inductances.The resistances were big enough so that the leak currents could be neglected. That way it was possible to run the model. However, for the models of the mutual inductances, the same problem occurred and, since no solution was found, the present simulations do not include that effect.

Another important point is that, to simplify the model and improve the simulation speed, a relay model for the anode and cathode regions were included, instead of the one described by Eqs. 3.12 and 3.13. This didn't bring significant differences to the model.

A typical electric arc

To show the main electric properties of the arcs, some simulations were performed without any disturbances and typical values of its parameters.

Figure 5.3 shows the simulated dynamic arc current-voltage characteristic, which can be compared with Figure 3.2. However, it only describes the voltage drop in the arc column. Therefore, in Figure 5.4 the anode and cathode voltage as a function of the current is plotted. By summing the arc column and the anode and cathode voltages we get the real current-voltage as in Figure 5.5. Figure 5.6 illustrates the delay of the anode and cathode voltage relatively to the arc current due to the capacitive effect in the anode and cathode regions.

Figure 5.7 shows the three arc voltages, with a relative shift of 120°. As can be seen, the arcs are ignited separately but we never have all of them extinguished at the same time. The arc currents are presented in Figure 5.8. The distortion is a consequence of the nonlinearity, as referred before. Their magnitudes are nearly 87 kA, corresponding to a secondary transformer current of $50kA$, which matches the data collected from Fundia.

Finally, the electrode voltages and currents are plotted in Figure 5.9. Again, the voltage is heavily distorted due to the harmonics from the arc. It must be pointed out that the currents are smother due to the low pass characteristics of the electric circuit, according to [Timm and Grigat, 1987].

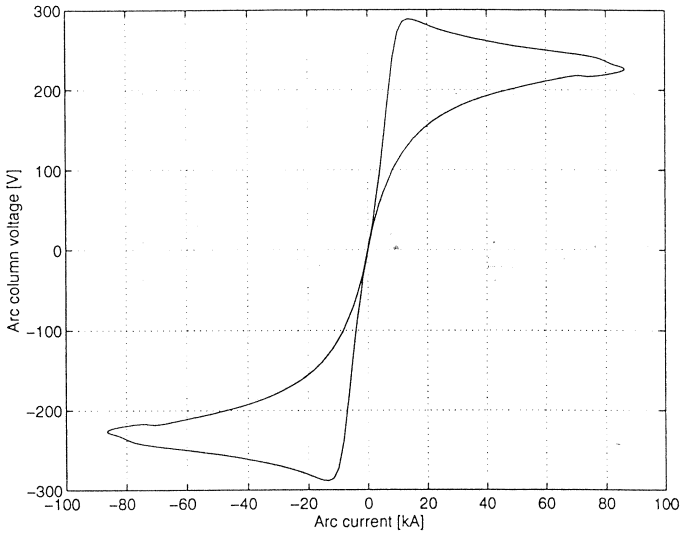

Figure 5.3 The dynamic arc column current-voltage characteristic

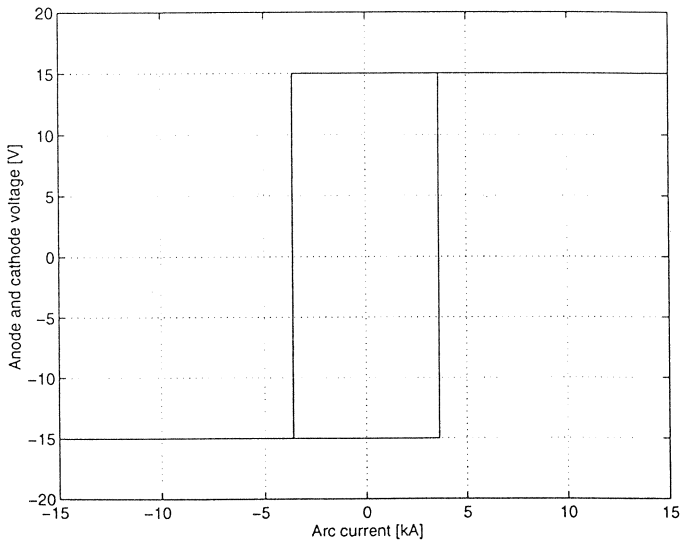

Figure 5.4 The anode and cathode voltage

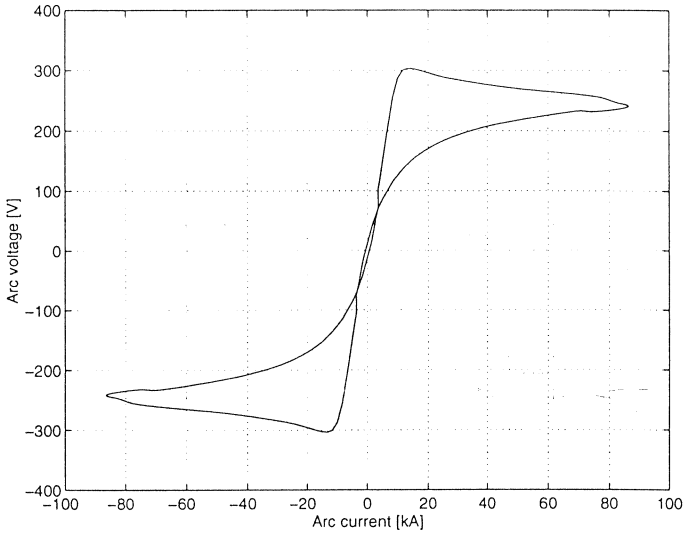

Figure 5.5 The dynamic arc current-voltage characteristic

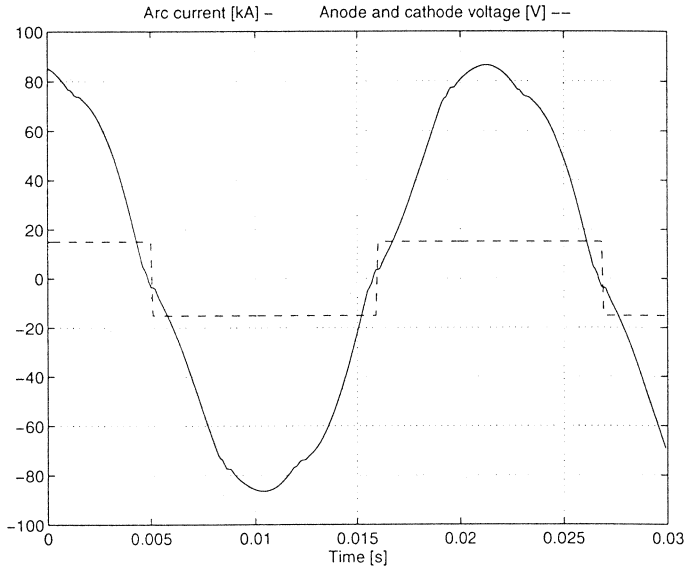

Figure 5.6 The anode and cathode voltage delay

The arc in the beginning of the process

In the beginning of the steel-melting process the conditions in the furnace are "cold" and so the plasma conductivity is lower. Therefore, the arc resistance is large which makes its ignition more difficult. Furthermore there is a large stochastic disturbance due to scrap movements and fast arc length variations. In this period, negative and positive polarity modes can be distinguished from each other since the respective arc voltages differ in shape and time to reach the firing voltage. Also as a consequence of the disturbances, the arcs sometimes get too long and, as a consequence, time intervals with nearly zero current occur, due to the fact that the arc takes more time to ignite.

Figure 5.10 captures the effects described. There, the arc voltage is heavily distorted. The arc current in Figure 5.11 has a very large variation in mag-

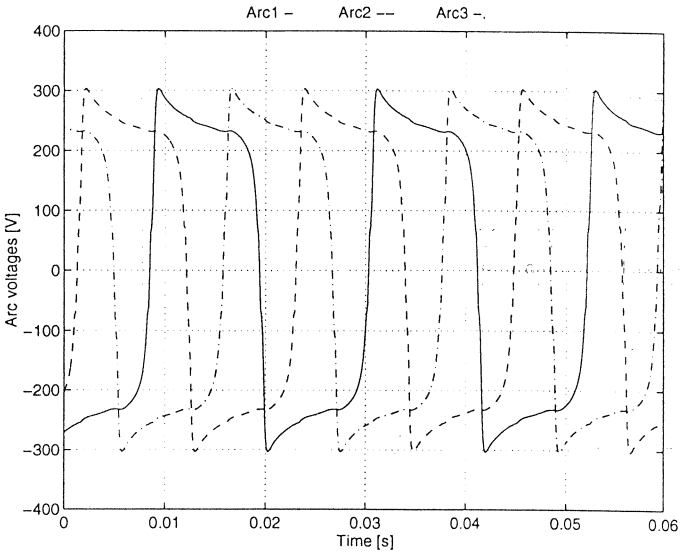

Figure 5.7 The arc voltages

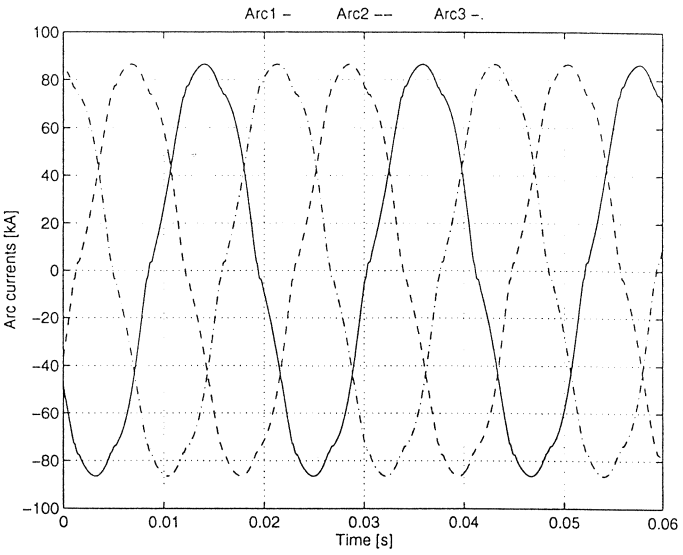

Figure 5.8 The arc currents

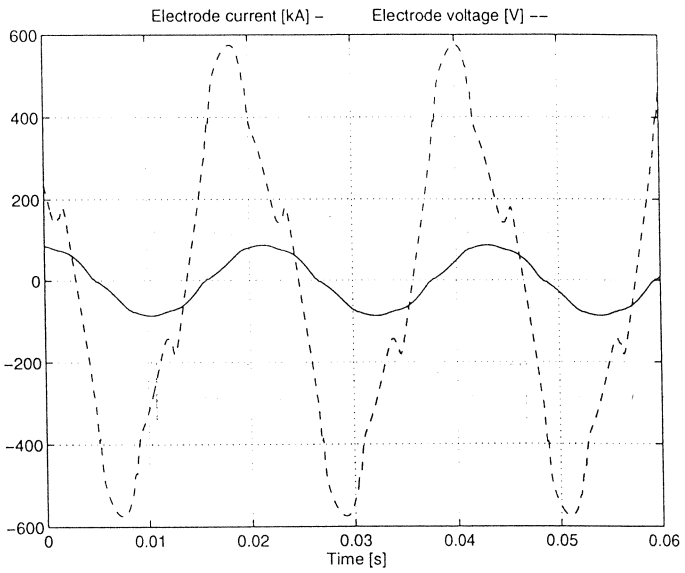

Figure 5.9 The electrode currents and voltages

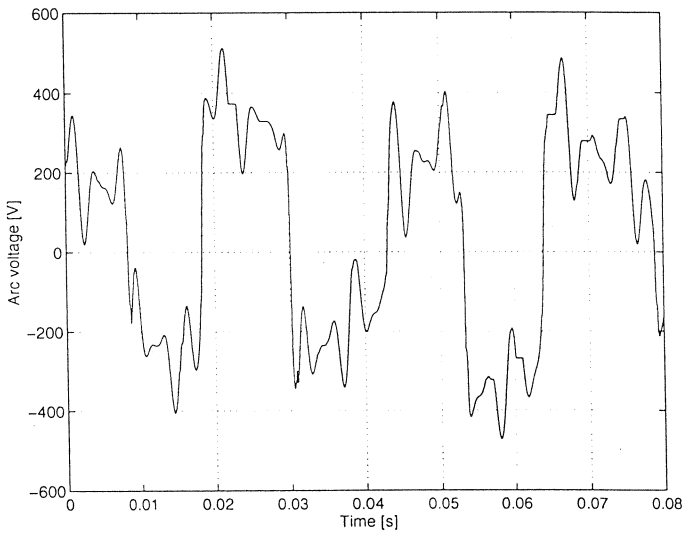

Figure 5.10 The arc voltage in the beginning of the process

nitude. It can be noted that in the periods when the current is low, which corresponds to a long arc, in the change of polarity there are time intervals with almost zero current.

The dynamic arc current-voltage characteristic in this period is plotted in Figure 5.12 and is, of course, strongly distorted. There, the repetitive pattern found in the arc voltage is a consequence of the high frequency sinusoidals used to model the disturbances.

The simulations presented can be compared with the results in [Timm and Grigat, 1987], displayed in Figure 5.13.

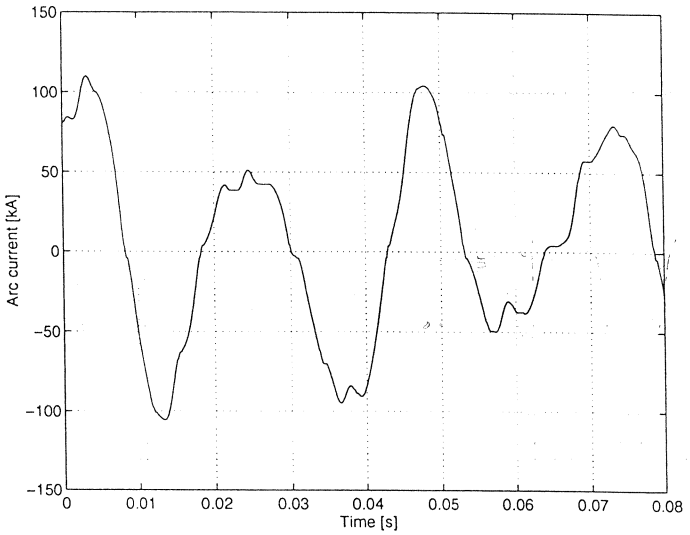

Figure 5.11 The arc currents in the beginning of the process

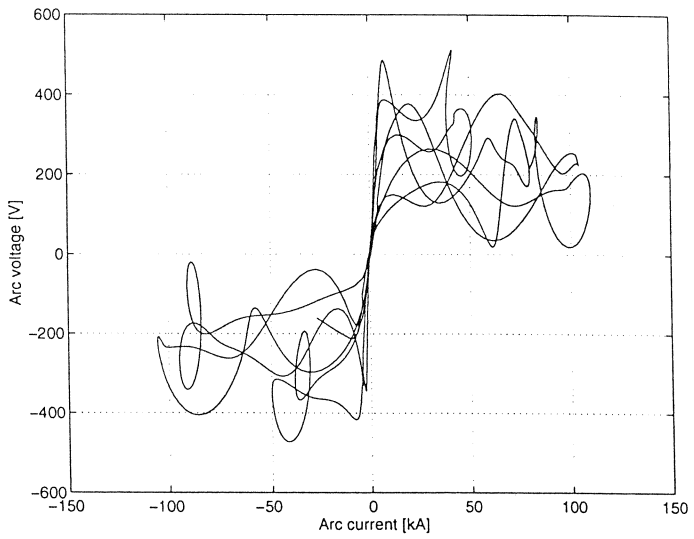

Figure 5.12 The dynamic arc current-voltage characteristic in the beginning of the process

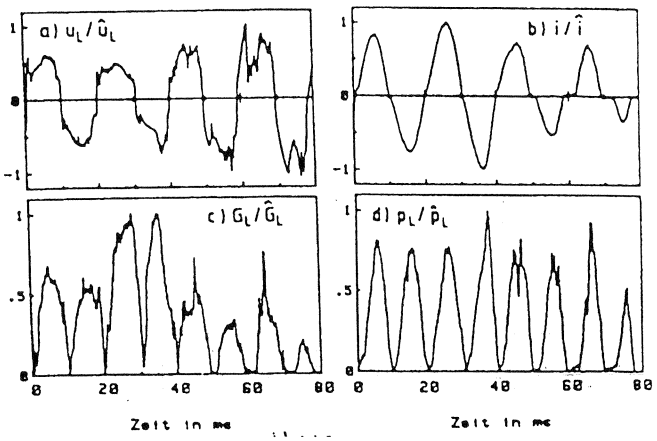

Figure 5.13 The arc in the beginning of the process

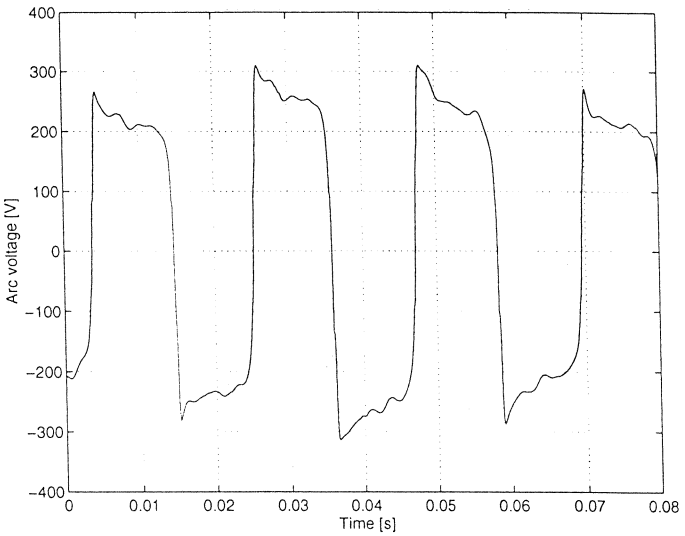

Figure 5.14 The arc voltage after 7 minutes

The arc after 7 minutes

7 minutes after the beginning the furnace conditions are described as "warm". The plasma conductivity is higher and the disturbances are much lower than in the beginning. Also the problem with arc ignition is much reduced.

Figure 5.14 shows the arc voltage. It is also somewhat distorted but, clearly, much less than in the beginning. At this time we also don't see time periods with zero current, according to Figure 5.15.

The dynamic characteristic in this period is plotted in Figure 5.16. The results obtained can be compared to the plots in Figure 5.17.

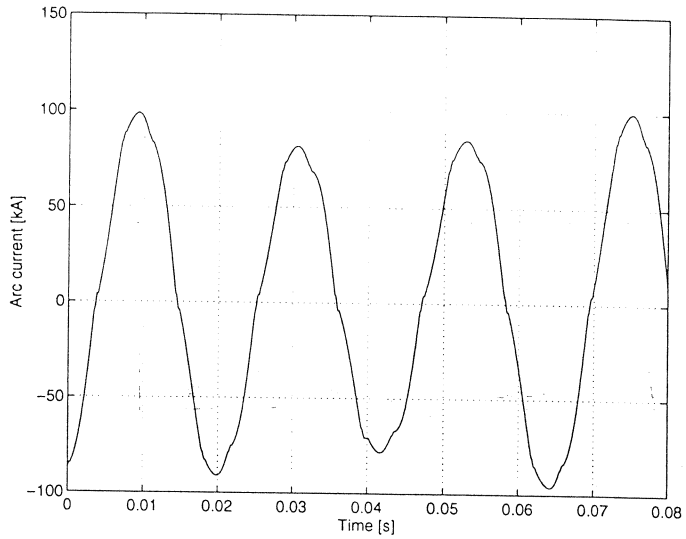

Figure 5.15 The arc currents after 7 minutes

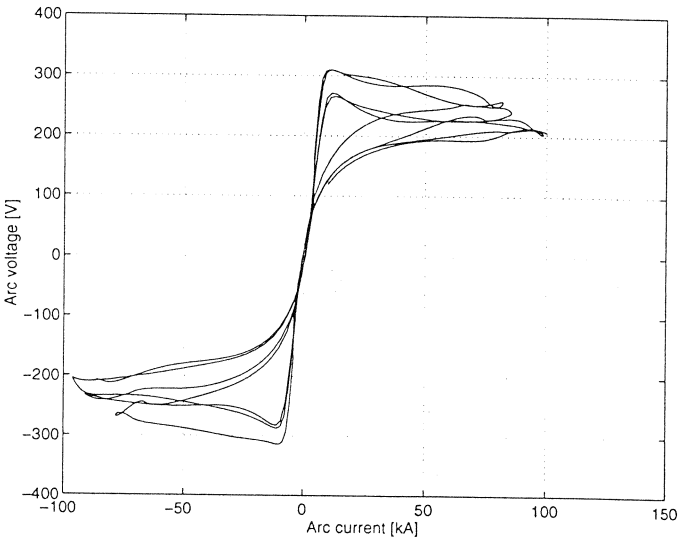

Figure 5.16 The dynamic arc current-voltage characteristic after 7 minutes

The arc after 27 minutes

27 minutes after the beginning we have a molten bath. This period is characterized by little stochastic context, similar positive and negative polarity modes and generally improved furnace conditions. The arc becomes an almost linear load which is demonstrated by Figures 5.18 and 5.19 where the arc voltage and current are almost sinusoidal. Figure 5.20 reflects this behavior. Figure 5.21 shows the results obtained in [Timm and Grigat, 1987].

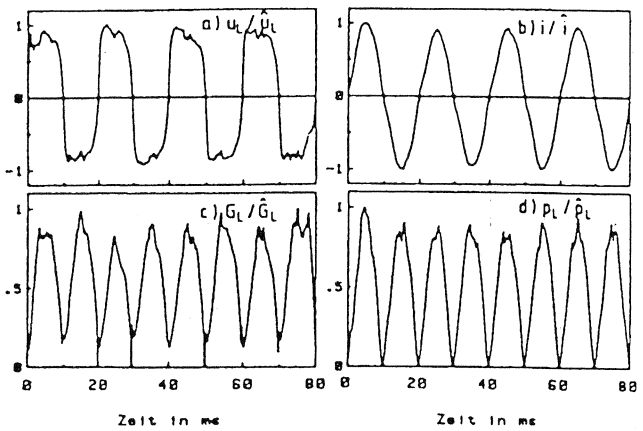

Figure 5.17 The arc after 7 minutes

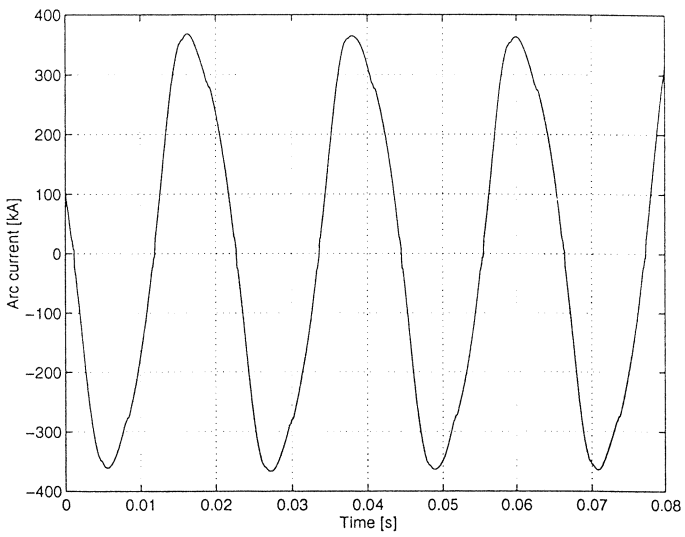

Figure 5.18 The arc voltage after 27 minutes

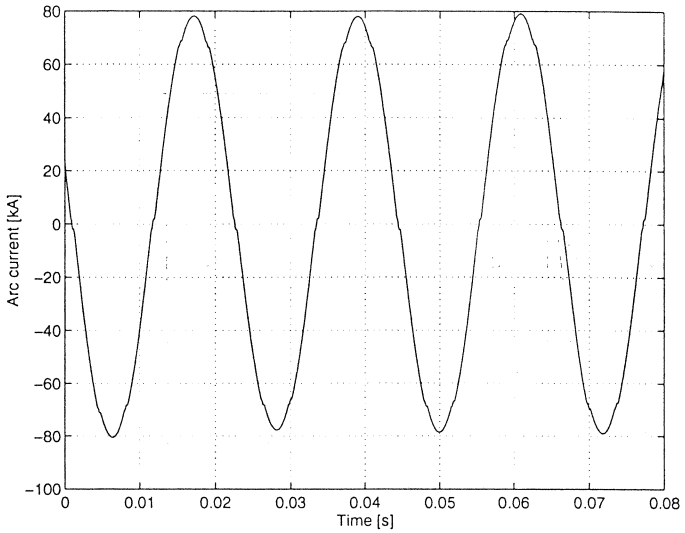

Figure 5.19 The arc currents after 27 minutes

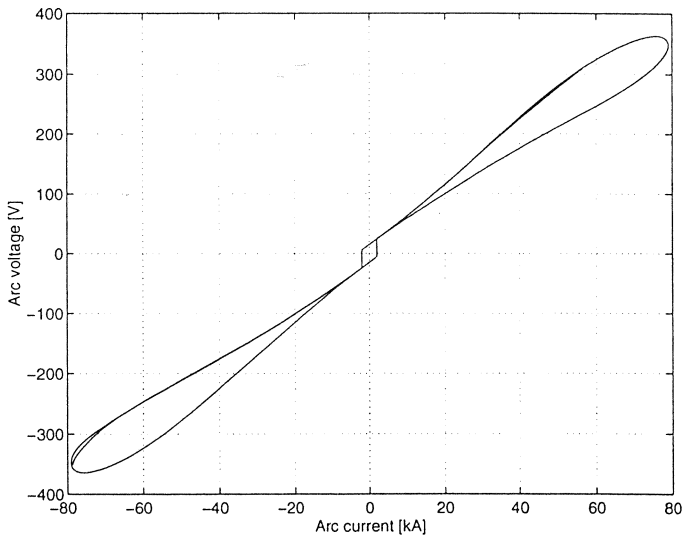

Figure 5.20 The dynamic arc current-voltage characteristic after 27 minutes

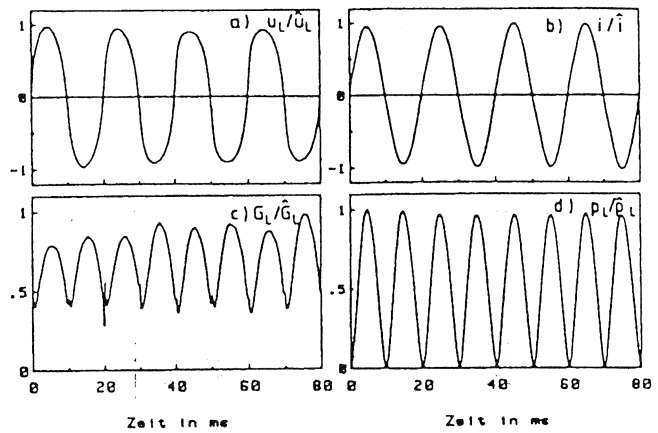

Figure 5.21 The arc after 27 minutes

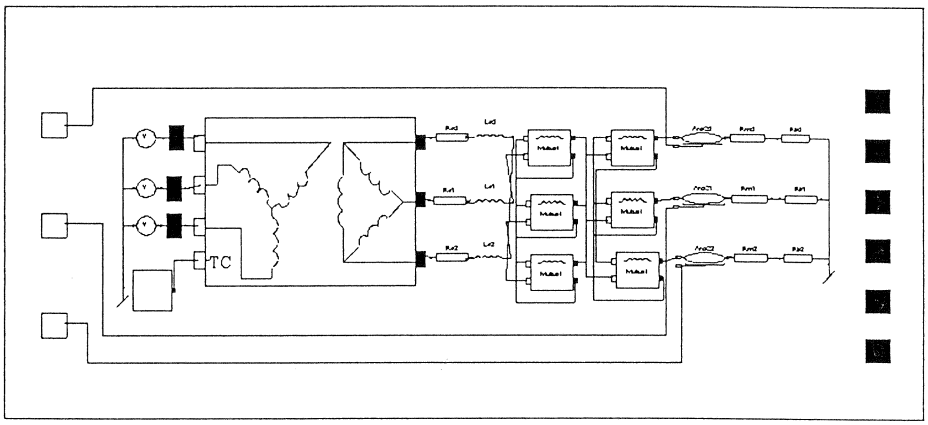

Figure 5.22 The EAF diagram for the steady-state model

5.2 The interaction effect

In order to simulate the interaction effects between phases, a steady-state model of the furnace electric system was used. Figure 5.22 shows the diagram used in Dymola. In these simulations also mutual inductances were included. As the goal of this section is to present the real effect, no disturbances were added.

In the simulations performed, one electrode is moved at one time and the effect in the currents is analyzed. The electrode displacement is the same for all the phases and equals $\pm 5cm$.

When electrode 1 is lowered (Figure 5.23) it can be seen in Figure 5.24 that its electrode current increases approximately $4kA$. Furthermore, the current in electrode 3 increases $2kA$ and the one in electrode 2 remains almost the same. When lifting electrode 1 the results are similar with the exception that the currents that increased in the opposite situation now decrease, according to Figure 5.26.

When lowering electrode 2, the increase in its current is accompanied by an increase in the one in electrode 1. The current in electrode 2 keeps the same value, as can be see in Figure 5.28. The effect of lifting electrode 2 is plotted

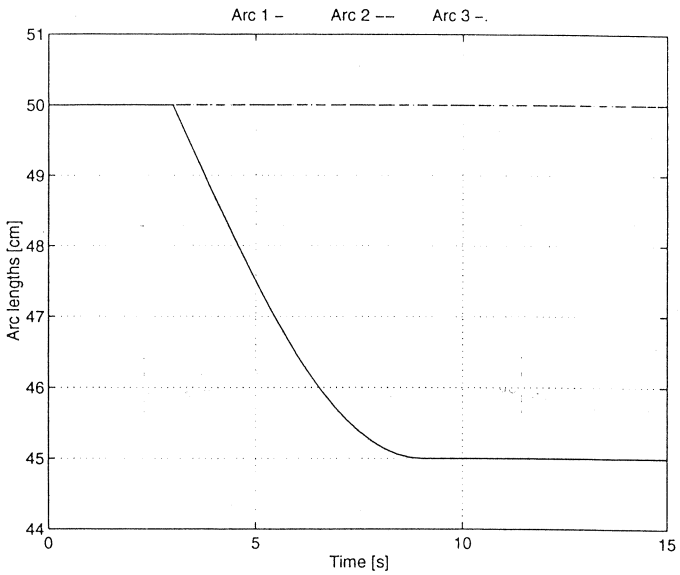

Figure 5.23 The arc lengths when lowering electrode 1

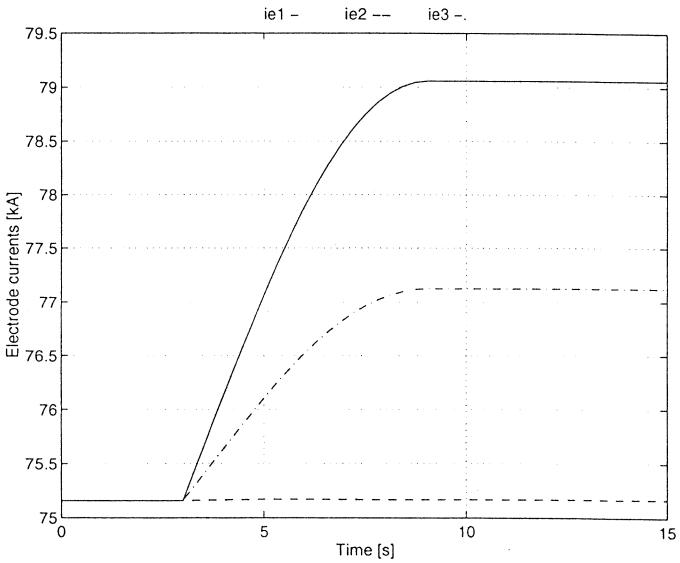

Figure 5.24 The electrode currents when lowering electrode 1

in figure 5.30.

Finally, lowering electrode 3 affects the current in this electrode and in electrode 2, according to Figure 5.32. Figure 5.34 shows the current variations when moving the electrode in the opposite direction.

As can be concluded by the results shown, with no disturbances, when moving one electrode the current in one of the other remains the same but the third electrode is highly affect by that movement. As a consequence the controller must compensate for this effect.

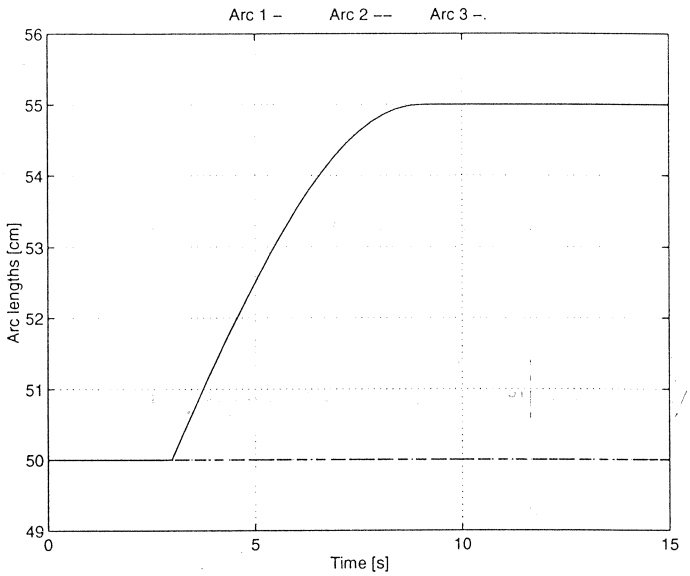

Figure 5.25 The arc lengths when lifting electrode 1

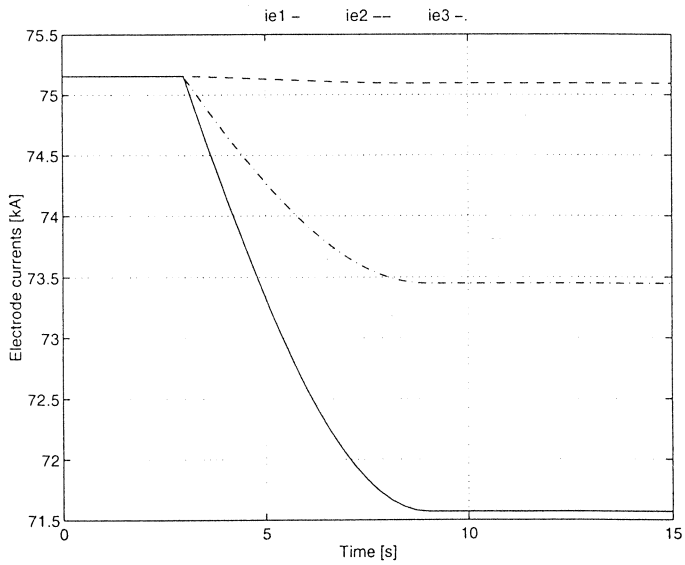

Figure 5.26 The electrode currents when lifting electrode 1

5.3 The effect of disturbances

In our model, the disturbances are represented by random variations in the arc lengths. The electrodes are lowered from $0.5m$ to $0.45m$ above the average scrap level, which moves randomly. Figures 5.35 and 5.36 show the arc lengths obtained and the respective arc currents. It can be seen that they vary a lot and, thus, efficient control is required.

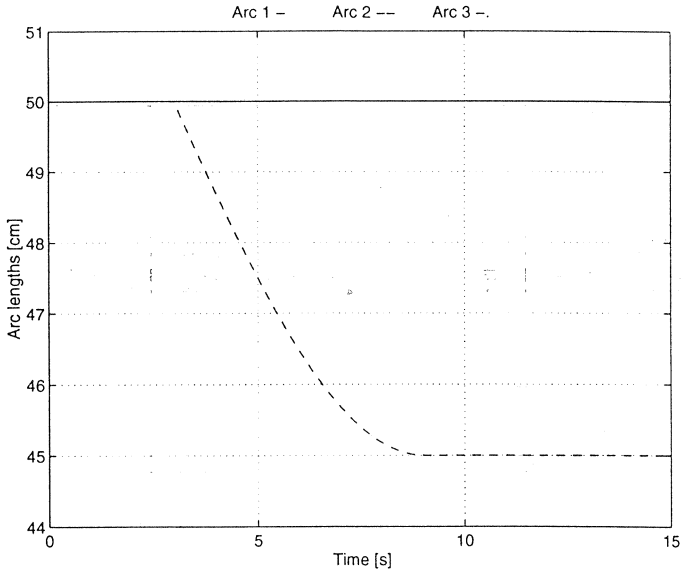

Figure 5.27 The arc lengths when lowering electrode 2

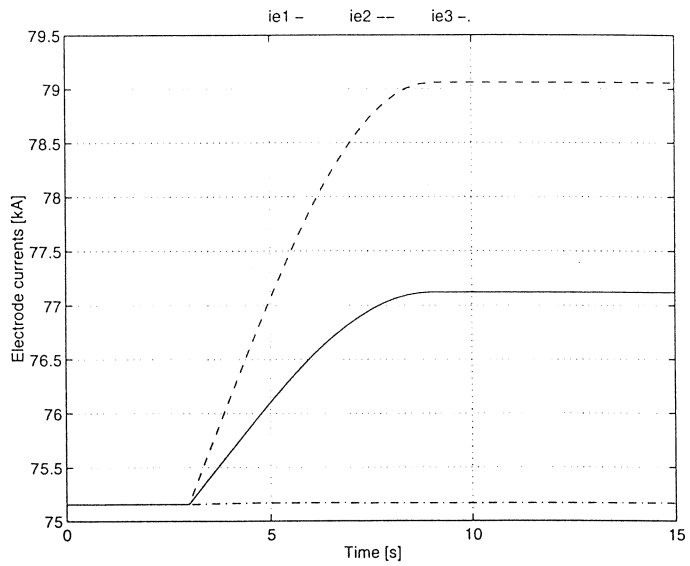

Figure 5.28 The electrode currents when lowering electrode 2

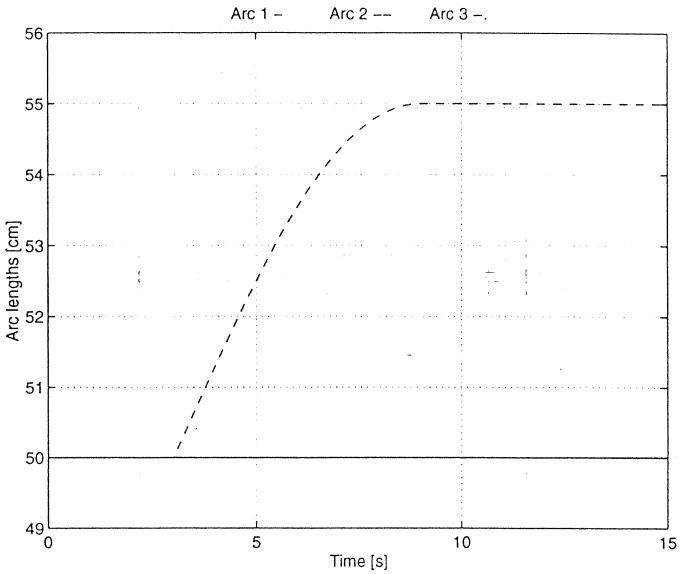

Figure 5.29 The arc lengths when lifting electrode 2

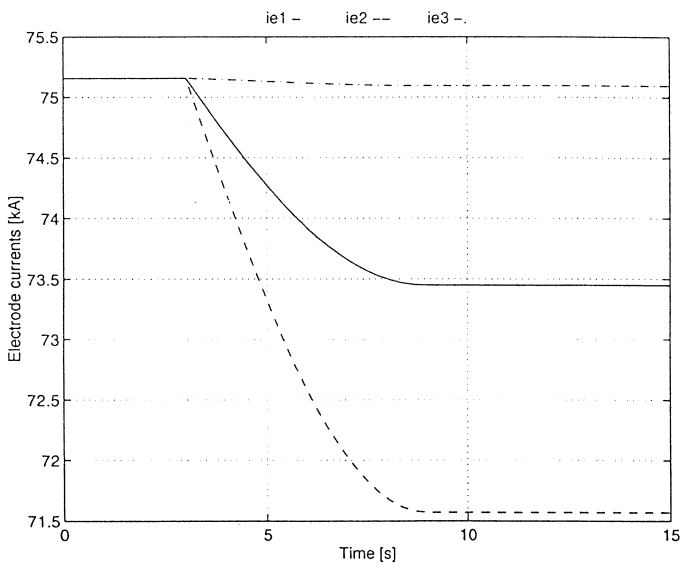

Figure 5.30 The electrode currents when lifting electrode 2

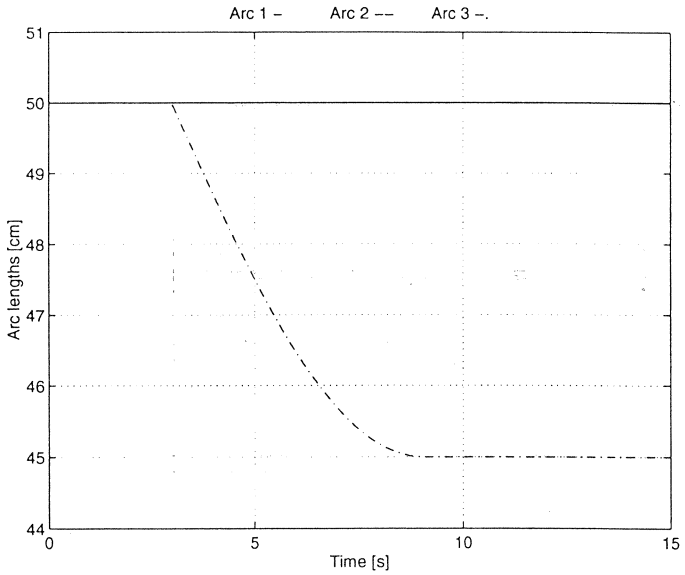

Figure 5.31 The arc lengths when lowering electrode 3

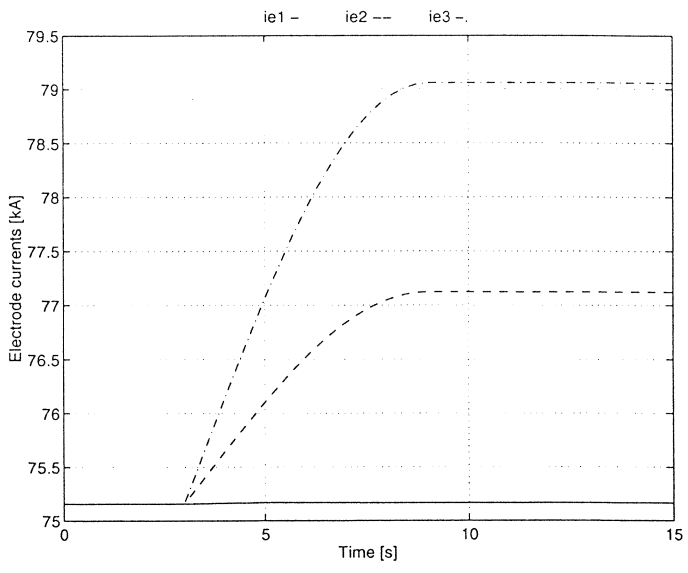

Figure 5.32 The electrode currents when lowering electrode 3

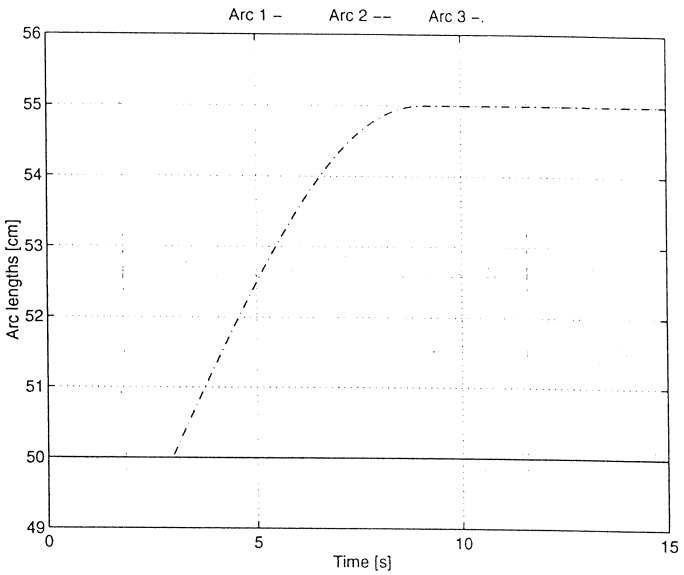

Figure 5.33 The arc lengths when lifting electrode 3

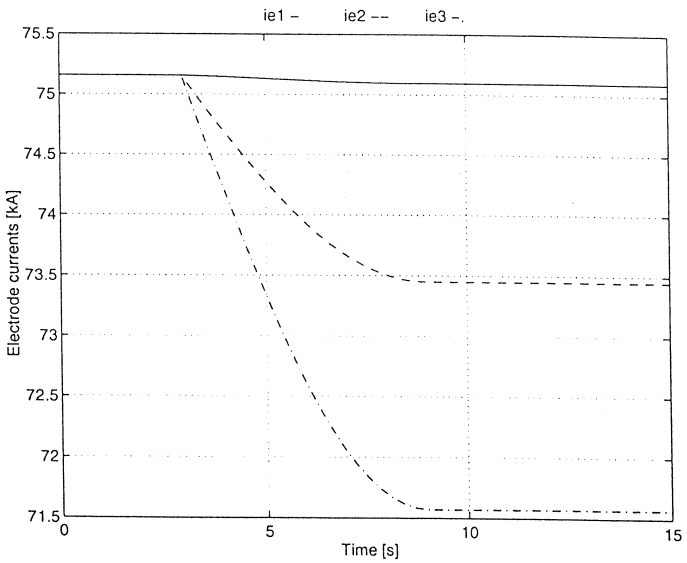

Figure 5.34 The electrode currents when lifting electrode 3

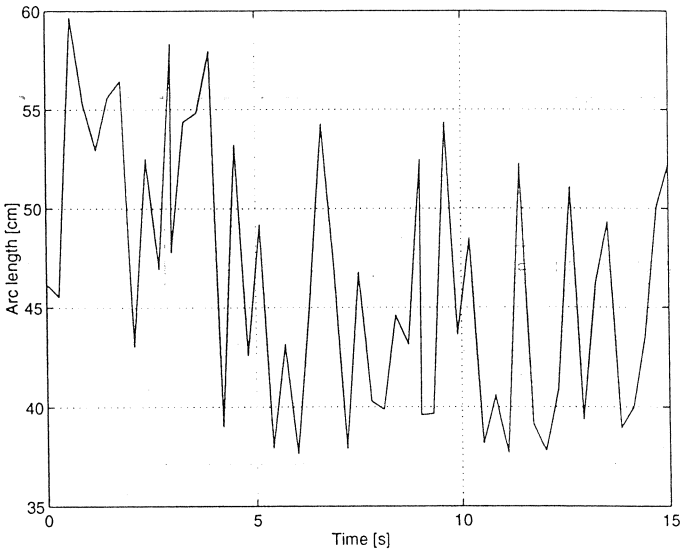

Figure 5.35 The effect of disturbances in the arc lengths

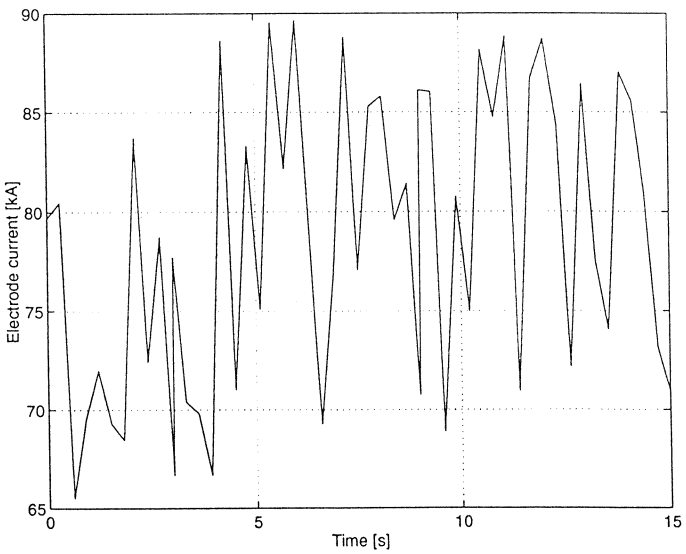

Figure 5.36 The effect of disturbances in the electrode currents

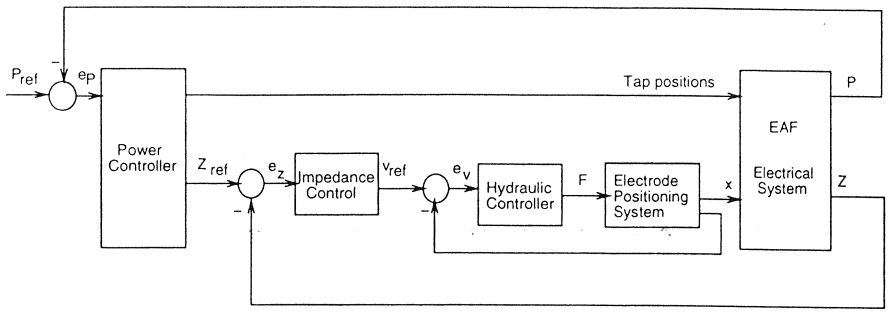

Figure 6.1 The EAF control system

6. The EAF Controller

In an EAF, electrical energy is the main source of energy required for the chemical reactions to take place. Thus, efficient electrical control is a main concern.

Figure 6.1 represents the EAF control system. As can be seen, we have three levels of control, namely *power control*, *impedance control* and *hydraulic control*. The power controller controls the delivered power to the furnace by calculating the reference levels for the phase impedances and the tap-changer positions. The impedance controller regulates the phase impedances by means of adjusting the arc lengths through electrode movements. The hydraulic controller controls the hydraulic forces generated by the hydraulic system to move the electrodes with the required speed references. In this chapter we will only shimmer the surface of power and hydraulic controllers since our main concern is impedance control.

6.1 Power control

During the steel-melting process there is a need to change the power supplied to the furnace. Generally, we need high power during the melt-down phase after which low power is used. As the power in the secondary circuit depends on the secondary voltage and current, it is important to control both of them.

As referred in Section 4.1, the secondary phase voltages can only be adjusted in discrete steps due to the nature of the transformer. In fact, the tap changer allows the selection of the ratio of the primary to the secondary voltage by selecting the number of coils in the primary side of the transformer. It turns out that the voltage can not be continuously adjusted.

Referring to current control, the electrode currents are controlled indirectly since the control principle is *regulate on constant impedance*, as will be seen in Section 6.2. The desired impedance is achieved through the electrode control mechanism. By adjusting the electrode position we change the arc length, its impedance and therefore we obtain a certain current.

High power is needed melt-down and so, the arc must be short in order to provide the necessary high currents. However, in this phase there is a significant variation of the arc length due to scrap movements, generating short circuits when scrap touches the electrodes. Thus, an efficient electrode positioning

control is required in order to achieve the desired arc length and, therefore, the power input level. When low power is needed, the electrodes are raised and thereby the arc length increases. As a result, the arc current decreases, as well as the arc power.

As a conclusion the main objectives of the power controller are to obtain the impedance references for the impedance control and select the tap-changer positions.

6.2 Impedance control

The goal of the impedance control is to drive the phase impedances to a desired set-point impedance. As referred above, the desired impedance is achieved by moving the electrodes. Lifting them, corresponds to increasing the arc length, and so, the phase impedance increases. Similarly, lowering the electrodes leads to a decrease in the phase impedance.

The phase impedances are calculated based on Root Mean Square (RMS) values of the electrode voltages and currents, as in Eq. 6.1. The measurements performed will be presented and discussed to some extent in Section 6.5.

$$Z = \frac{U_{RMS}}{I_{RMS}} \tag{6.1}$$

Control problems

When controlling the EAF electrical system several problems can be encountered. The major ones are the following:

1. **Large stochastic disturbances**
   The major disturbances to the arc lengths, mainly in the melt-down phase, can be seen as the most important control problem. Therefore, a very efficient control is desired in this phase.

2. **The dynamics of the electrode positioning system**
   When the electrode positioning system is slow, efficient impedance control is difficult to achieve. Furthermore, if the knowledge about the positioning system is limited, it is difficult to determine if the cause of an unsatisfactory control is a bad design of the impedance controller or bad electrode positioning dynamics.

3. **Electrode currents are not controlled**
   Since the electrode currents are not controlled, they can go beyond the operational current constraints. However, the power control is responsible for keeping all electrical variables within bounds.

4. **Unreliable measurements**
   As will be discussed later the voltage measurements are somewhat unreliable. Thus, the calculated impedances will differ from the real values.

5. **The interaction effects between phases**
   According to [Valderhaug, 1992], the interaction effect between the control loops is negligible when using impedance control. However, if a current controller is used instead of a impedance controller, there will be significative interaction between the control loops. To handle this problem, a decoupler could be used.

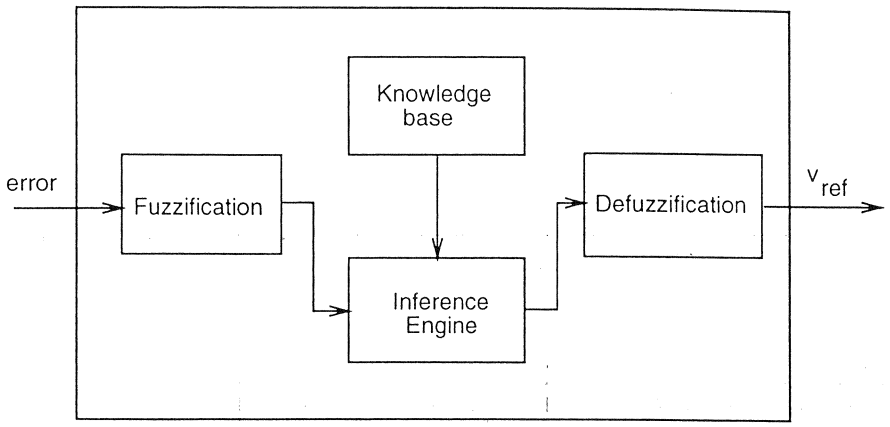

Figure 6.2 The fuzzy logic controller system

6. **Asymmetry in the three-phase system**
   In a real furnace, the phase impedances are not equal. Furthermore, due to geometrical asymmetry, the mutual inductances between phases are also different. These situations leads to a more complex interaction effect.

6.3 A Fuzzy P-like impedance controller

One of the goals of this thesis was to design a fuzzy impedance controller. It would be interesting to design a PI-like controller. However, due to unexpected numerical problems with Dymola, it was not possible. Therefore, a P-like fuzzy controller was used. As will be seen later, the desired non-linearity in the proportional gain is easily obtained with this controller. In this section, the structure of the controller, namely the knowledge base, the inference engine and the fuzzification and defuzzification units presented in Figure 6.2, will be described.

The knowledge base

According to [Johansson and Årzén, 1996], a fuzzy knowledge base consists of fuzzy IF-THEN rules and membership functions characterizing the fuzzy sets.

The **rule base** consists of seven rules, as follows.

where e denotes the impedance deviation and v_{ref} is the controller output

IF	e	IS	NB	THEN	v_{ref}	IS	NB
IF	e	IS	NM	THEN	v_{ref}	IS	NM
IF	e	IS	NS	THEN	v_{ref}	IS	NS
IF	e	IS	ZE	THEN	v_{ref}	IS	ZE
IF	e	IS	PS	THEN	v_{ref}	IS	PS
IF	e	IS	PM	THEN	v_{ref}	IS	PM
IF	e	IS	PB	THEN	v_{ref}	IS	PB

and denotes the electrode speed references. The labels NB, NM, NS, ZE, PS,

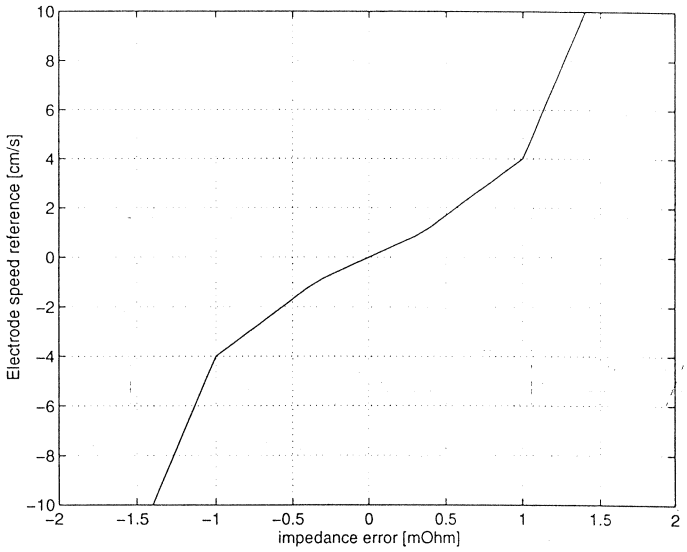

Figure 6.3 The proportional gain nonlinearity

PM and PB mean *Negative Big*, *Negative Medium*, *Negative Small*, *Zero*, *Positive Small*, *Positive Medium* and *Positive Big*, respectively. The **membership functions** used are triangular functions. This class of membership functions is characterized by its simplicity and easy computation. According to documentation from ABB, the proportional gain should be defined as follows. For an error of $\pm 5\%$ the control output should be $\pm 5\%$ of the maximum value. For an error of $\pm 50\%$ the speed reference should be around $\pm 40\%$ of the maximum. For an error higher than 70% the output should be maximum. Notice that in the impedance controller the upwards and downwards gains are equal. The assymetry of the positioning system is taken care of by the hydraulic controller. Figure 6.3 shows the proportional gain nonlinearity obtained. This kind of nonlinearity is approximately a quadratic function of the error, $e \cdot |e|$, and it is useful to reduce the sensitivity to measurement noise. This nonlinearity was obtained by defining the membership functions for the error and speed reference as in Figure 6.4.

The resulting knowledge base presented is called a *complete*, *consistent information system* .

Fuzzification

Since the knowledge base is defined, the next step is to apply the fuzzification operation, i. e., to transform the numeric inputs into membership values. In our case, a the numeric value of the impedance error is mapped into membership values, through the triangular membership functions. Thus, for each linguistic term from Negative Big to Positive a degree of fulfillment is obtained.

The inference engine

After the mapping of the numeric values of the error into fuzzy sets, it is time to infer the output of the controller. This goal is performed by the inference engine. It is this element of the fuzzy controller that performs all fuzzy logic manipulations.

The inference engine used is the *Min-Max inference engine*. In order to reason with our seven rules, individual rule base inference is used. From each

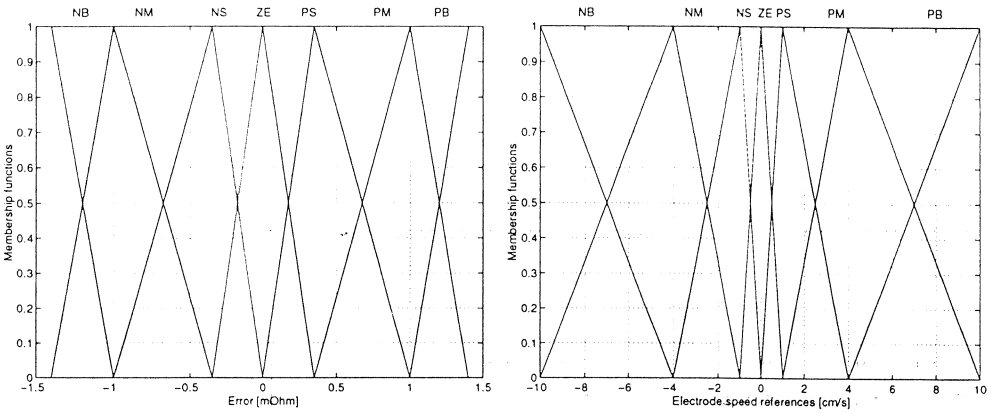

Figure 6.4 The membership functions for the error and speed references

rule an output fuzzy set is inferred by using min as the implication operator. Then the total output is obtained by combining all the individual fuzzy sets using the max operator. Notice that, since the controller only has one input, in this case the antecedents do not need to be computed.

Defuzzification

As the output of the inference engine is a fuzzy set, it is necessary to transform it into a numeric value. This operation is called fuzzification.

The defuzzifier used is the *Center Average*. The numeric value is computed as the weighted average of the centers of the individual consequents fuzzy sets, as follows:

$$v_{ref} = \frac{\sum_{i=1}^{n} c_i \cdot w_i}{\sum_{i=1}^{n} w_i} \tag{6.2}$$

There, c_i stands for the centers of the individual consequent fuzzy sets. w_i denotes the weight of each fuzzy set and is equal to the membership value of each antecedent. n is the number of rules, in this case equal to seven.

6.4 Hydraulic control

In order to have satisfactory control, the hydraulic controller plays a very important role. The hydraulic forces applied to the electrode arms must be accurate so that the electrode speed references are obtained. An important point here is that, due to considerable electrode weights, a higher force must be used when moving them upwards. Furthermore, since the hydraulic force is limited, the maximum downward speed is higher than the one in the opposite direction. However, as referred before, the knowledge concerning the electrode positioning system is very limited. Thus, the complete hydraulic control system can be modelled as in Section 4.3 and repeated here:

$$\frac{h_a(s)}{v_{ref}(s)} = \frac{1}{s} \cdot \frac{1}{Ts+1} \tag{6.3}$$

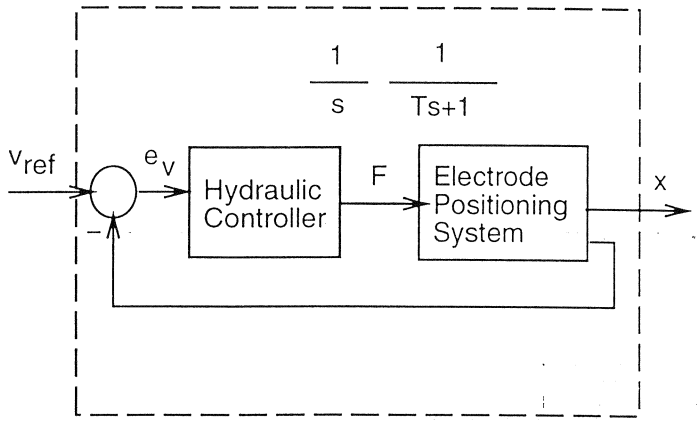

Figure 6.5 The hydraulic control system

This structure is due to the fact that in our furnace the outputs of the controller are the electrode speed references and not the electrode positions. The speed references are used because, due to large contents of disturbances, electrode consumption and varying bath nature, it is difficult to relate the electrode positions to the arc lengths. It seems more reasonable to give the speed and direction to which the electrodes should be moved and not what position they should be moved to. The maximum downward and upwards velocities can be captured by including an assymetric saturation in the model.

6.5 Measurements

In this section, the way the measurements are performed in the steel mill at Smedjebacken will be described and analyzed.

Electrode voltages

In the vicinity of the furnace secondary circuit there is a very high magnetic field due to the high secondary currents. This results in induced voltages in any electrode circuit close to the furnace. As a consequence, special care is necessary when measuring the electrode voltages. A simple voltage measurement between the electrodes and the furnace bottom can not be used because the measured voltages will consist of both the electrode voltages and the induced ones. However, according to [Valderhaug, 1992], in open-arc furnaces the induction effects can be compensated. In Smedjebacken, a measurement transformer is used to compensate for the referred induction phenomenon.

Electrode currents

To measure the electrode currents directly on the electrodes is difficult due to the very high currents on the secondary side. Making this kind of measurements requires special equipment and, thus, a common way to handle this problem is to measure the currents in the primary side.

In Fundia, the transformer tap-changer position is compensated for by the use of an intermediate current transformer. However, measuring the currents in the primary side of the transformer has the problem that it is difficult to make the correspondence between the currents measured and the electrode

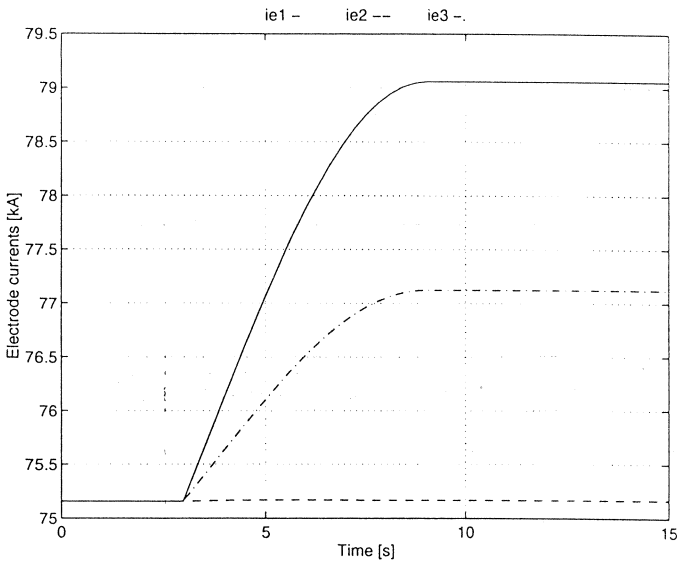

Figure 6.6 The electrode currents when lowering electrode 1

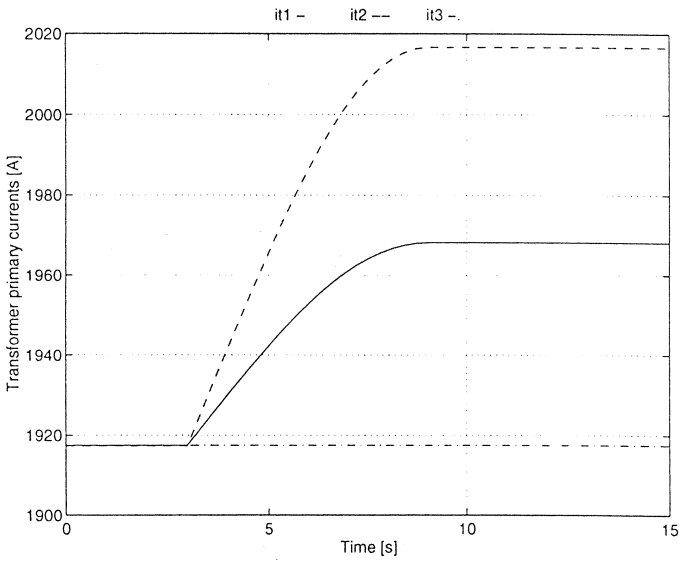

Figure 6.7 The corresponding transformer primary voltages

currents. For instance, Figure 6.6 shows that electrode 1 has the highest current but in Figure 6.7 this is not true. Therefore, according to [Valderhaug, 1992], the measurements circuit must be arranged in a delta-star circuit, as in the furnace. In this way, the electrode currents will be directly proportional to the ones measured.

Data logging

According to [Jansson, 1995] the measured currents and voltages are taken from the measurement equipment to an adjustable voltage divider and then to a transducer. The transducer transfers the measured data to an analogue input which is connected to the data logger system ARGUS. All data is stored

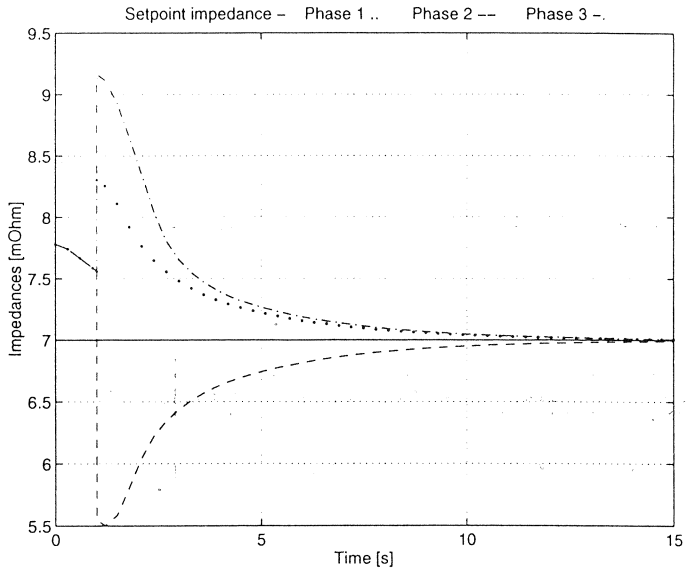

Figure 6.8 The controlled phase impedances for a step disturbance

as RMS values, according to:

$$U = \sqrt{\frac{1}{T}\int u(t)^2} \tag{6.4}$$

where U denotes the RMS value for a time varying variable $u(t)$ and T denotes the integration time. The sample interval was approximately $3Hz$.

6.6 Control simulations

The controller described was implemented in Dymola as a discrete controller, with a sampling time of $0.3sec$, as in Fundia. The response of the system to step and to stochastic disturbances were simulated.

Figure 6.8 shows the controlled phase impedances when the arc lengths are subject to a step disturbance. As can be seen, the system can follow the reference impedance with no steady-state error. Since the nonlinear proportional gain is small, there is no overshoot. The control actions, shown in Figure 6.9, are high for larger impedance deviations after what they become lower, as it was expected. The consequent arc lengths are plotted in Figure 6.10.

When the arc lengths are subjected to random disturbances, the system can not follow the set-point impedance. This was somewhat expected since, for strong stochastic disturbances, the arc length has large instantaneous variations. Thus, even with a very fast electrode positioning system, the set-point impedance can not be followed. However, as displayed in Figure 6.11, the phase impedance has an average value that is equal to the set-point impedance. As a consequence of the random disturbances, the control signal varies much more compared to step disturbances, according to Figure 6.12. Figure 6.13 shows the highly variating arc lengths.

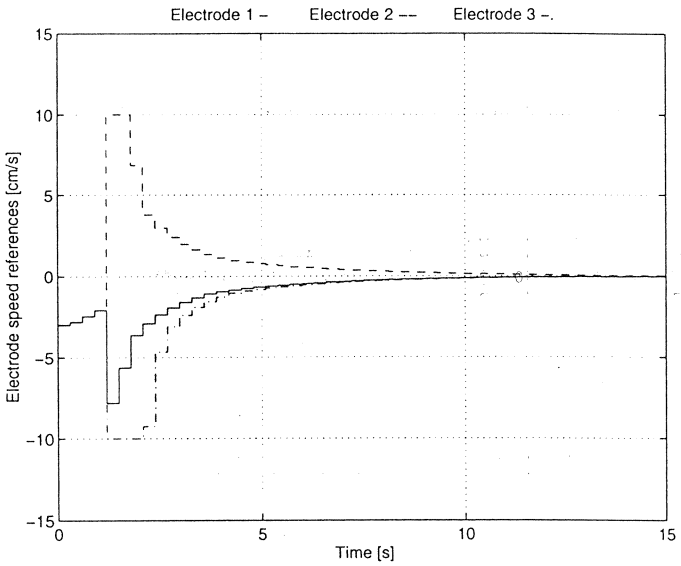

Figure 6.9 The control signals for a step disturbance

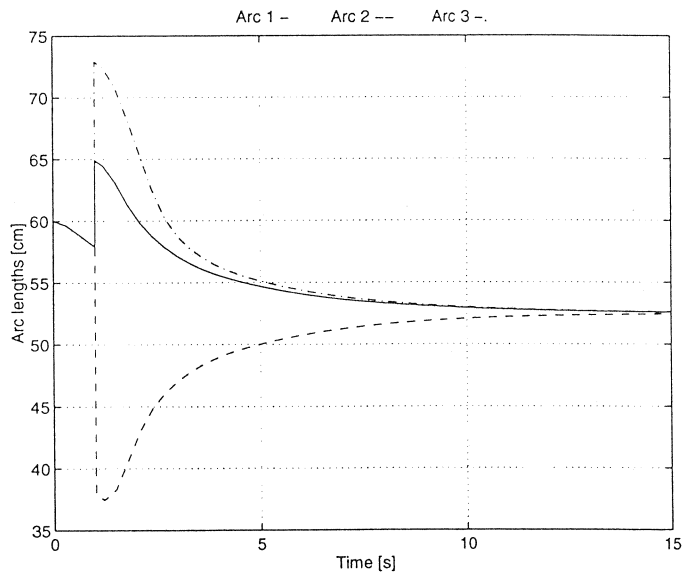

Figure 6.10 The arc lengths for a step disturbance

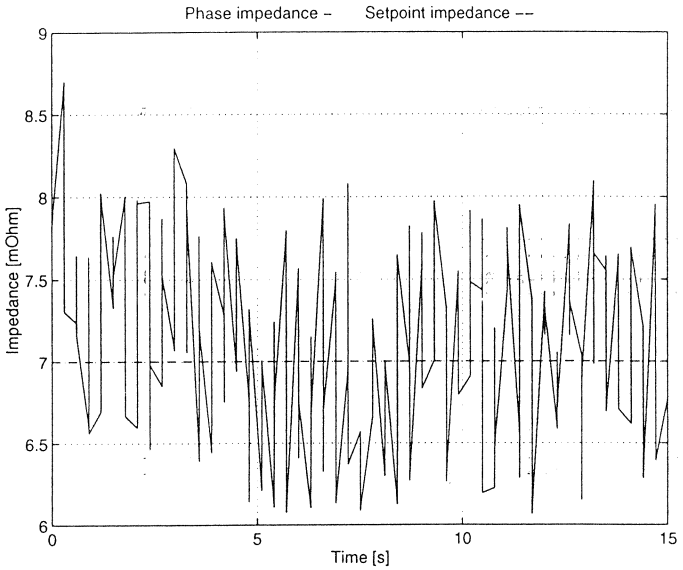

Figure 6.11 The controlled phase impedances for a random disturbance

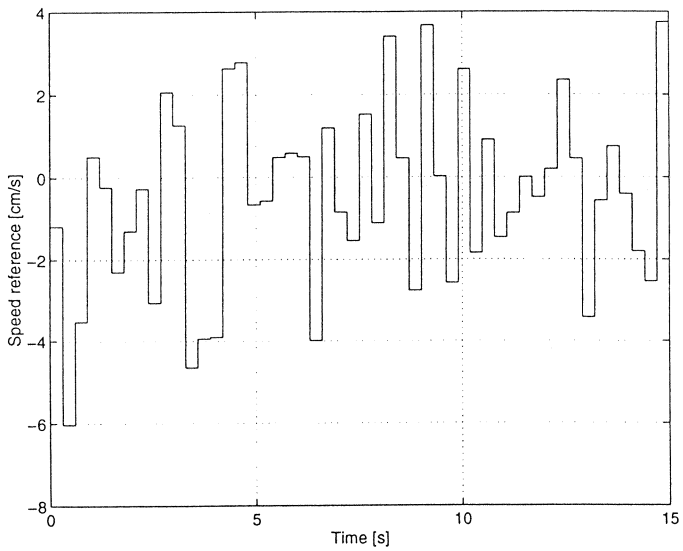

Figure 6.12 The control signals for a random disturbance

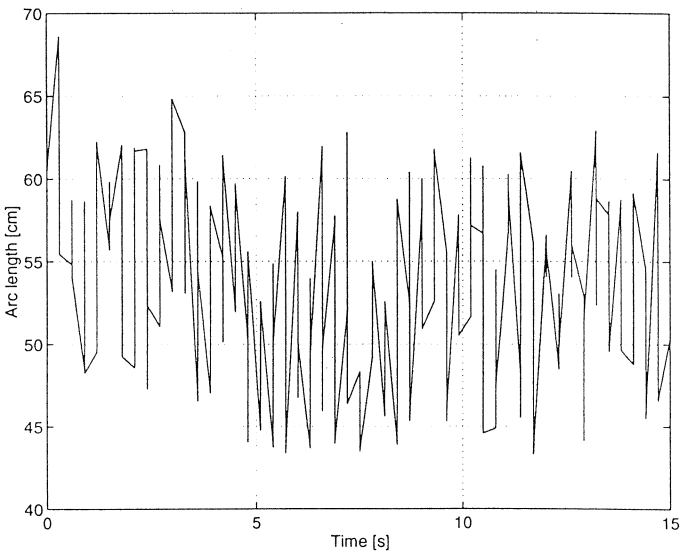

Figure 6.13 The arc lengths for a random disturbance

7. Conclusions

7.1 Contributions of the thesis

The purpose of this thesis was to implement a physical model of an Electric Arc Furnace and design a fuzzy logic impedance controller.

To attain the first goal, an object-oriented model of the EAF was developed. The major advantage of this object-oriented model is its modularity. In this way, more flexibility in changing parts of the system is attained, since each submodel can be modified separately without affecting the overall structure. Models of the furnace three-phase generator, transformer, electrode positioning dynamics, disturbances and the EAF electrical system were included. In the electrical system, two models of the electric arc, namely the Cassie and Köhle arc models, were presented. A model of the electrode mutual inductances were also implemented. Furthermore, both a dynamic and a steady-state model were developed, by the reasons presented before. The electrical conditions during the furnace operation were analyzed and simulated.

The other purpose was to design a fuzzy impedance controller. A fuzzy P-like controller was presented and its behavior was discussed.

7.2 Limitations of the thesis

During the implementation of the model and the controller some problems were encountered and some assumptions were made due to lack of knowledge.

Referring to the electrical system, some parameters were based on data from [Valderhaug, 1992]. Probably these are typical values for EAF but it would be better to know the real values in the furnace in Smedjebacken.

The electrode positioning system is poorly understood. Since it plays a vital role in the control, it is very important to have more knowledge about this system.

The nature of the disturbances to the process should be better understood in order to design an efficient impedance controller.

In order to have an accurate comprehension of the interaction effect between phases, the mutual inductances between them must be analyzed. A suggestion for measurements that should be performed is given.

When performing simulations some problems were found. The dynamic model constituted a high-index DAE. To overcome this problem, high resistances were included in parallel with the electrode self-inductances. However, it was not possible to include the electrode mutual inductances in this model. In the steady-state model, algebraic loops were present, which slowed down the simulations. In order to improve the simulation time, so-called tearing could be used. In [Elmqvist and Otter, 1994], methods for tearing are presented.

Referring to the controller, it was not possible to design a fuzzy PI-like controller due to numerical problems with Dymola. Furthermore, the discrete time controller used is, of course, very slow, as a consequence of the generation of events required to sample. Also, other control strategies, such as current control, could be analyzed.

8. Bibliography

BILLINGS, S. A. (1981): *Modelling and identification of a three-phase electric-arc furnace.*, chapter 3, pp. 63–80. IEE, Institution of Electrical Engineers, London and New York.

BROWNE, T. E. (1955): "The electric arc as a circuit element." *Journal of the Electrochemical Society*, **102:1**, pp. 27–37.

ELMQVIST, H. and M. OTTER (1994): "Methods for tearing systems of equations in object-oriented modeling.". ESM'94 European Simulation Multiconference.

HAUKSDÓTTIR, A. S., T. SÖDERSTRÖM, Y. P. THORFINNSON, and A. GESTSSON (1995): "System identification of a three-phase submerged-arc furnace." *IEEE Transactions on Control Systems Technology*, **3:4**, pp. 377–387.

JANSSON, P. (1995): "On tunning of fuzzy logic controllers applied to an electric arc furnace.". Master's thesis, Royal Institute of Technology, Stockholm.

JOHANSSON, M. and K.-E. ÅRZÉN (1996): "A primer on fuzzy control." Technical Report, Department of Automatic Control, Lund, Sweden.

KÖHLE, S. (1992): "Lineares ersatzschaltbild des drehstrom-lichtbogenofens für die betriebliche anwendung des kreisdiagramms." Seminar notes: Electrotechnik des Lichtbogenofens. in German.

TIMM, V. K. and R.-R. GRIGAT (1987): "Rechnergestützte prozebßeobachtung des schmelzvorganges im lichtbogenofen." *Electrowärme International*, **B 1:45**, pp. 29–36. in German.

VALDERHAUG, A. M. (1992): *Modelling and control of submerged-arc ferrosilicon furnaces.* PhD thesis Report 92-81-W, Norwegian Institute of Technology, Trondheim.

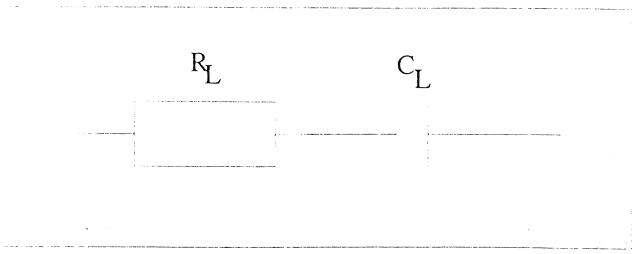

Figure A.1 The electric arc modeled as a capacitive load

A. Köhle's model

A.1 Relating Cassie's and Köhle's models

Arc voltage magnitude analogy

In order to find a relation between the linear and the nonlinear model, the difference in the arc voltages given by each of them should be minimized:

$$min(|v_{aC}| - |v_{aK}|) = min(R_a ia + v_a + v_c - Z_L ia) \approx min(R_a - |Z_L|) \quad \text{(A.1)}$$

where v_{aK} represents the arc voltage given by Köhle and v_{aC} represents Cassie's arc voltage.

That minimization can be achieved by letting $|Z_L|$ be equal to the average value of R_a:

$$|Z_L|\frac{T}{2} = \int_0^{\frac{T}{2}} R_a(t)dt$$
$$|Z_L| = f(\tau_a, E_0, h_a) \quad \text{(A.2)}$$

where T represents the period of current and voltage waves.

Phase analogy

If the arc is interpreted as a inductive load, its voltage will lead the current. But, according to Cassie's model, there is a capacitive effect which delays the anode and cathode voltages compared to the arc current. Thus, it seems more reasonable to interpret the arc as a capacitive load, as seen in Figure A.1. The arc phase is shown in Figure A.2.

A.2 The effect of changes in the arc length in Köhle's model

The magnitude of the arc impedance

As can be concluded from Cassie's model, the arc resistance, R_a, is nearly

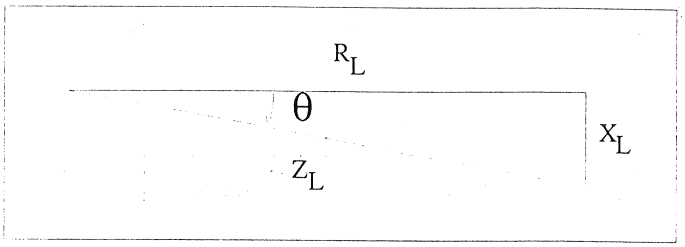

Figure A.2 The arc phase

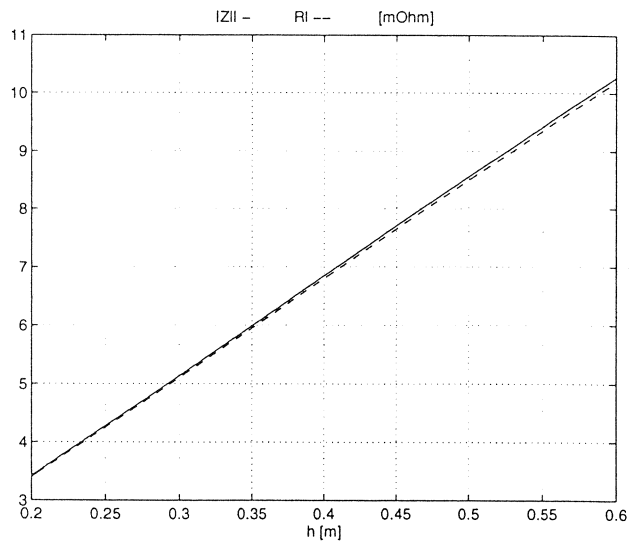

Figure A.3 The arc impedance as a function of the arc length

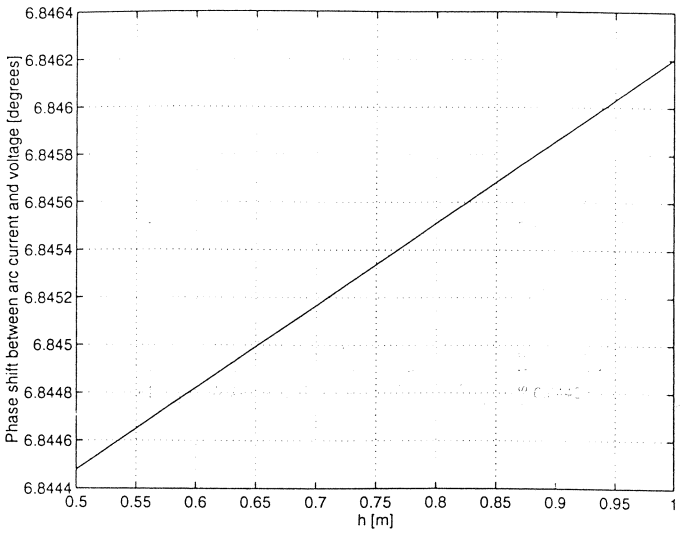

Figure A.4 The arc phase as a function of the arc length

directly proportional [1] to the arc length, h_a. According to the relation between this model and the linear one described above, one can conclude that the same happens for the arc impedance:

$$h_{a2} = mh_{a1} \Rightarrow |Z_{L2}| \simeq m|Z_{L1}| \tag{A.3}$$

where Z_{Li} is the impedance when the arc length is h_{ai}.

Making $R_L = h\hat{R}_L$ we obtain:

$$Z_L = h\hat{R}_L\sqrt{1 + a^2 + 2abh\hat{R}_L + (bh\hat{R}_L)^2} \tag{A.4}$$

$$Z_L \simeq h\hat{R}_L \tag{A.5}$$

$$Z_L \simeq R_L \tag{A.6}$$

which corresponds to the fact that the arc is almost a pure resistive load. The conclusions presented are supported by Figure A.3. The parameters used to simulate it are the ones given by table B.7.

The arc phase

Figure A.4 shows that the arc phase variation with the length is nearly linear. Furthermore, we can also say that it is almost constant.

$$\theta \simeq 6.84^\circ \tag{A.7}$$

From Eq. A.5 we can relate the arc phase with the arc length= which allows as to write the following expression for the phase variation:

$$\theta = \cos^{-1}\sqrt{1 + a^2 + 2abh\hat{R}_L + (bh\hat{R}_L)^2} \tag{A.8}$$

[1] In fact, changing the arc length also changes the current and R_a depends on it. However, that change doesn't influence significantly what was said.

B. Simulation parameters

Table B.1 gives the parameters for the furnace electrical system used throughout the simulations. The relation between the transformer ratio and the tap-changer position for a primary voltage of $20kV$ is presented in Table B.2, adopted from [Jansson, 1995]. Tables B.3, B.4, B.5 and B.6 give Cassie's arc parameters for the situations simulated, as described in Section 5.1. Finally, Table B.7 presents Köhle's arc parameters used in the steady-state model.

The value $\hat{R}_L$ was obtained based on [Timm and Grigat, 1987]. There, it is said that the typical arc voltage per length unit $\hat{V}_L$ is $1000V/m$. Thus, for a typical arc current of $87kA$ we obtain:

$$|\hat{Z}_L| = 11.5m\Omega$$
$$\hat{R}_L \simeq 11.5m\Omega$$

Transformer primary voltage	V_P $[kV]$	20
Tap Changer Position	LK	22
Transformer resistances	R_T $[m\Omega]$	0.03
Transformer inductances	L_T $[mH]$	0.001
Electrode resistances	R_{ei} $[m\Omega]$	0.1
Electrode inductances	Lei $[mH]$	0.011
Metal bath resistances	R_{mi} $[m\Omega]$	0.11
Bottom resistances	R_{bi} $[m\Omega]$	0.32
Mutual inductances	M_{ij} $[mH]$	0.001

Table B.1 The model parameters used during the simulations

Tap-Changer Position	Transformer ratio	Secondary voltage [V]
11	35.292	566.7
12	33.5683	595.8
13	31.8296	628.4
14	31.6406	632.1
16	29.3902	680.5
17	28.2606	707.7
18	27.1297	737.2
19	26.0112	768.9
20	24.8787	803.9
21	23.7586	841.8
22	22.6296	883.8

Table B.2 The relation between the tap-changer position and the transformer ratio

Electric fields in DC arc	E_{0i}	$[V/m]$	450
Time constants	τ_{ai}	$[ms]$	0.5
Arc lengths	h_{ai}	$[m]$	0.5
Anode voltages	V_{Ai}	$[V]$	15
Cathode voltages	V_{Ci}	$[V]$	-15
Currents for voltage alternation	Δi_{ai}^{+}	$[kA]$	3.6
	Δi_{ai}^{-}	$[kA]$	-3.6

Table B.3 Cassie's arc parameters for a typical arc

Electric fields in DC arc	E_{0i}	$[V/m]$	600
Time constants	τ_{ai}	$[ms]$	0.3
Anode voltages	V_{Ai}	$[V]$	15
Cathode voltages	V_{Ci}	$[V]$	-15
Currents for voltage alternation	Δi_{ai}^{+}	$[kA]$	4
	Δi_{ai}^{-}	$[kA]$	-4

Table B.4 Cassie's arc parameters in the beginning of the process

Electric fields in DC arc	E_{0i}	$[V/m]$	550
Time constants	τ_{ai}	$[ms]$	0.4
Anode voltages	V_{Ai}	$[V]$	15
Cathode voltages	V_{Ci}	$[V]$	-15
Currents for voltage alternation	Δi_{ai}^{+}	$[kA]$	4
	Δi_{ai}^{-}	$[kA]$	4

Table B.5 Cassie's arc parameters 7 minutes after

Electric fields in DC arc	E_{0i}	$[V/m]$	500
Time constants	τ_{ai}	$[ms]$	10
Arc lengths	h_{ai}	$[m]$	0.5
Anode voltages	V_{Ai}	$[V]$	15
Cathode voltages	V_{Ci}	$[V]$	-15
Currents for voltage alternation	Δi_{ai}^{+}	$[kA]$	2
	Δi_{ai}^{-}	$[kA]$	-2

Table B.6 Cassie's arc parameters 27 minutes after

Arc resistance per length unit	$\hat{R}_L$	$[m\Omega/m]$	11.5
Arc reactance parameters	a		0.12
	b		0.02

Table B.7 Köhle's arc parameters used during steady-state model simulations

C. Dymola libraries

C.1 Dynamic model library

Cassie's arc model

```
model class ArcCassie
  cut a  (Va/i)
  cut b  (Vb/-i)
  cut a1  (h)
  main cut mc [a,  b]
  main path mp <a - b>

  parameter E0=100 Tc0=0.001
  parameter va=7.5 vc=-7.5 iap=7.2E3 iam=-7.2E3

  local Ralu=0.01 Ra=1 vcol Varc
  local vac

  der(Ralu) = 1/Tc0 * (1 - (Ralu*i/E0)**2) * Ralu
  Ra=Ralu*h
  Ra*i = vcol

  when i>iap or i<iam then
    vac = if i>iap then va else vc
  endwhen

  Varc = vcol + vac
  Varc = Va - Vb
end
```

Single-phase transformer

```
model class SPTransf
  cut Ap (Vpa/ipr)
  cut Bp  (Vpb/-ipr)
  cut As (Vsa/isc)
  cut Bs  (Vsb/-isc)

  parameter N=40

  Vpa - Vpb = N * (Vsa -Vsb)
  ipr = 1/N * isc
end
```

Tap-changer

```
model class TapChanger
  cut B (N)
```

```
  parameter LK[22]=[40, 40, 40, 40, 40, 40, 40, 40, 40, 40, ->
35.292, 33.5683, 31.8269, 31.6406, 30.5, 29.3902, 28.2606, ->
27.1297, 26.0112,24.8787,23.7586, 22.6296]

  {N= if Time<3 then LK(11) else LK(22) }
  N=LK(22)
end
```

EAF transformer

```
model class EAFTransf
  cut C3  (V3 /i3)
  cut C1  (V1/i1)
  cut C2  (V2/i2)
  cut A1  (V1p/i1p)
  cut A3  (V3p/i3p)
  cut A2  (V2p/i2p)

  parameter Rt=0.03E-3 Lt=0.001E-3

  submodel (ResistorI) Rt2  (R=Rt)
  submodel (ResistorI) Rt3  (R=Rt)
  submodel (ResistorI) Rt1  (R=Rt)
  submodel (InductorI) Lt2  (L=Lt)
  submodel (InductorI) Lt1  (L=Lt)
  submodel (InductorI) Lt3  (L=Lt)
  submodel (SPTransf) SPTr1
  submodel (SPTransf) SPTr2
  submodel (SPTransf) SPTr3
  submodel (GroundI) G

  connect Rt2:a at Lt2:b
  connect Lt3:b at Rt3:a
  connect Lt2:a at C2
  connect Rt1:a at Lt1:b
  connect A1 at SPTr1:Ap
  connect A3 at SPTr3:Ap
  connect A2 at SPTr2:Ap
  connect SPTr1:Bs at Lt2:a
  connect SPTr1:As at Rt1:b
  connect SPTr3:As at Rt2:b
  connect SPTr3:Bs at Lt3:a
  connect SPTr2:As at Rt3:b
  connect SPTr2:Bs at Lt1:a
  connect Lt3:a at C3
  connect Lt1:a at C1
  connect G:a at SPTr1:Bp
  connect SPTr3:Bp at G:a
  connect SPTr2:Bp at G:a
end
```

Electrode Positioning System

```
model class ElPosDynamics
  cut B3 (h3)
  cut A3 (vref3)
  cut B1 (h2)
  cut A1 (vref1)
  cut B2 (h1)
  cut A2 (vref2)

  submodel (StateSpace) stateSpace3 ->
   (A=[-4 0; 1 0], B=[1;0], C=[0 4], D=[0])
  submodel (StateSpace) stateSpace1 ->
   (A=[-4 0; 1 0], B=[1;0], C=[0 4], D=[0])
  submodel (StateSpace) stateSpace2 ->
   (A=[-4 0; 1 0], B=[1;0], C=[0 4], D=[0])

  connect A3 at stateSpace3:in
  connect stateSpace3:out at B3
  connect stateSpace1:out at B1
  connect stateSpace1:in at A1
  connect stateSpace2:in at A2
  connect stateSpace2:out at B2
```

Disturbances

```
model class Disturbances
  cut B1 (dh1)
  cut B3 (dh3)
  cut B2 (dh2)

  parameter d=5

  dh1 = (RandomUniform(Time) - 0.5) /d
  dh2 = (RandomUniform(Time) - 0.5) /d
  dh3 = (RandomUniform(Time) - 0.5) /d
end
```

C.2 Steady-state model library

Electrical components

```
model class TwoPinP
  cut a {* CutA at (-105, -5) (-95, 5)} (Va_d Va_q/ I_d I_q)
  cut b {* CutB at (95, -5) (105, 5)} (Vb_d Vb_q/ -I_d -I_q)
  main cut  mc [a, b]
  main path mp <a -b>

  constant pi  = 3.141593 f0  = 50 om0 = 2*pi*f0

  local U_d U_q
```

```
  U_d = Va_d - Vb_d
  U_q = Va_q - Vb_q
end

model class (TwoPinP) InductorP
  parameter L

  U_d = -om0*L*I_q
  U_q = om0*L*I_d
end


model class (TwoPinP) CapacitorP
  parameter C

  U_d = I_q/(C*om0)
  U_q = -I_d/(C*om0)
end


model class (TwoPinP) VsourceP
  Terminal V0 Ph

  - V0 * cos(Ph)  = U_d
  V0 * sin(Ph)  = U_q
end

model class (TwoPinP) I_RMSP
  local I_RMS

  I_RMS = sqrt (I_d**2 + I_q**2)

  U_d = 0
  U_q = 0
end
```

Köhle's arc model

```
model class ArcKohleSS
  cut a (Va_d Va_q/ I_d I_q)
  cut b (Vb_d Vb_q/ -I_d -I_q)
  cut a1 (h)
  main cut mc [a,  b]
  main path mp <a - b>

  constant pi=3.14159 f0=50 om0=2*pi*f0

  parameter a = 0.12 b = 0.02 Rllu = 11.5E-3

  submodel (ResistorPv) Rl
  submodel (CapacitorPv) Cl
```

```
  connect Rl:b at Cl:a
  connect Rl:a at a
  connect Cl:b at b

  Rl.R = h * Rllu
  Cl.C = 1 / (om0 * (a*Rl.R + b*Rl.R**2) )
end
```

Mutual Inductances

```
model class MutIndSS
  cut A1 (Va1_d Va1_q/ I1_d I1_q)
  cut A2 (Va2_d Va2_q/ I2_d I2_q)
  cut B1 (Vb1_d Vb1_q/ -I1_d -I1_q)
  cut B2 (Vb2_d Vb2_q/ -I2_d -I2_q)
  main cut mc [A1, B1]
  main path mp <A1 -B1>

  constant pi  = 3.141593 f0  = 50 om0 = 2*pi*f0

  parameter M

  local U_d U_q

  Va2_d - Vb2_d = 0
  Va2_q - Vb2_q = 0
  U_d = Va1_d - Vb1_d
  U_q = Va1_q - Vb1_q
  U_d = -om0*M*I2_q
  U_q = om0*M*I2_d
end
```

C.3 Controller

Discrete controller

```
model class DiscControl
  parameter SamplingRate=0.3

  local NextTime = 0 ed1=0 ed2=0 ed3=0

  cut Ae3 (e3)
  cut Ae1 (e1)
  cut Ae2 (e2)
  cut B3 (vref3)
  cut B1 (vref1)
  cut B2 (vref2)

when Time>NextTime then
  new(NextTime)=NextTime+SamplingRate
```

```
  new(ed1)=e1
  new(ed2)=e2
  new(ed3)=e3

  new(vref3)=p_fuzzy_ctrl(new(ed3))
  new(vref1)=p_fuzzy_ctrl(new(ed1))
  new(vref2)=p_fuzzy_ctrl(new(ed2))
endwhen
end
```

Control C function

```
float p_fuzzy_ctrl (float e){
  float ve[ME], vdu[MDU], ant[ME], u, numer, denom;
  int rule[ME], i;

  ve[NB]=-0.0014; ve[NM]=-0.001; ve[NS]=-0.00035; ve[ZE]=0;
  ve[PS]=0.00035; ve[PM] = 0.001; ve[PB]=0.0014;
  vdu[NB]=-10; vdu[NM]=-4.0; vdu[NS]=-1; vdu[ZE]=0; vdu[PS]=1;
  vdu[PM]=4.0; vdu[PB]=10;

  rule[NB] = NB;
  rule[NM] = NM;
  rule[NS] = NS;
  rule[ZE] = ZE;
  rule[PS] = PS;
  rule[PM] = PM;
  rule[PB] = PB;

  if (e<ve[NB]) ant[NB]=1;
  else ant[NB] = triangular(ve[NB]-1,ve[NB],ve[NM],e);
  ant[NM] = triangular(ve[NB],ve[NM],ve[NS],e);
  ant[NS] = triangular(ve[NM],ve[NS],ve[ZE],e);
  ant[ZE] = triangular(ve[NS],ve[ZE],ve[PS],e);
  ant[PS] = triangular(ve[ZE],ve[PS],ve[PM],e);
  ant[PM] = triangular(ve[PS],ve[PM],ve[PB],e);
  if (e>ve[PB]) ant[PB]=1;
  else ant[PB] = triangular(ve[PM],ve[PB],ve[PB]+1,e);

  numer=0; denom=0;
  for (i=0;i<ME;i++) {
      numer = numer + ant[i]*vdu[rule[i]];
      denom = denom + ant[i];
    }

  u=(numer/denom)/100; /* convert centimeters to meters*/

  return u;
```